

การสังเคราะห์และพิสูจน์เอกลักษณ์อนุภาคคาร์บอนนาโนที่ได้จากการเผาไหม้พาราฟิน



นางสาวเยาวพา สารจันทร์

ศูนย์วิทยทรัพยากร  
จุฬาลงกรณ์มหาวิทยาลัย

วิทยานิพนธ์นี้เป็นส่วนหนึ่งของการศึกษาตามหลักสูตรปริญญาวิทยาศาสตรมหาบัณฑิต

สาขาวิชาปิโตรเคมีและวิทยาศาสตร์พอลิเมอร์

คณะวิทยาศาสตร์ จุฬาลงกรณ์มหาวิทยาลัย

ปีการศึกษา 2552

ลิขสิทธิ์ของจุฬาลงกรณ์มหาวิทยาลัย

SYNTHESIS AND CHARACTERIZATION OF CARBON NANOPARTICLES BY  
PARAFFIN COMBUSTION

Miss Yaowapa Sarajan




ศูนย์วิทยทรัพยากร  
จุฬาลงกรณ์มหาวิทยาลัย

A Thesis Submitted in Partial Fulfillment of the Requirements  
for the Degree of Master of Science Program in Petrochemistry and Polymer Science  
Faculty of Science  
Chulalongkorn University  
Academic Year 2009  
Copyright of Chulalongkorn University

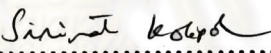
Thesis Title                                   SYNTHESIS AND CHARACTERIZATION OF CARBON  
  NANOPARTICLES BY PARAFFIN COMBUSTION  
By   Miss Yaowapa Sarajan  
Field of Study                                 Petrochemistry and Polymer Science  
Thesis Advisor                                 Associate Professor Dr. Sanong Ekgasit

---

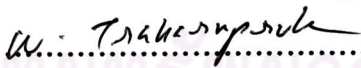
Accepted by the Faculty of Science, Chulalongkorn University in Partial  
Fulfillment of the Requirements for the Master's Degree

  
.....Dean of the Faculty of Science  
(Professor Supot Hannongbua, Dr. rer. nat.)

THESIS COMMITTEE

  
..... Chairman  
(Associate Professor Sirirat Kokpol, Ph.D.)

  
..... Thesis Advisor  
(Associate Professor Sanong Ekgasit, Ph.D.)


  
..... Examiner  
(Associate Professor Wimonrat Trakarnpruk, Ph.D.)

  
..... External Examiner  
(Assistant Professor Toemsak Srihirin, Ph.D.)

เขาวพา สารระจันทร: การสังเคราะห์และพิสูจน์เอกลักษณะอนุภาคคาร์บอนนาโนที่ได้จากการเผาไหม้พาราฟิน. (SYNTHESIS AND CHARACTERIZATION OF CARBON NANOPARTICLES BY PARAFFIN COMBUSTION) อ.ที่ปริกษาวิทยานิพนธ์หลัก : รศ. คร. สนอน เอกสิทธิ์, 78 หน้า.

ในการศึกษาอนุภาคระดับนาโนเมตรของคาร์บอนสังเคราะห์โดยวิธีการเผาไหม้ของพาราฟิน นำพาราฟินมาขึ้นรูปเป็นเทียนไข และใช้เป็นแหล่งกำเนิดของคาร์บอน ได้ศึกษาปัจจัยต่างๆที่มีผลต่อการสังเคราะห์อนุภาคระดับนาโนเมตรของคาร์บอน ปัจจัยที่เหมาะสมทั้งหมดนี้สามารถสังเคราะห์อนุภาคระดับนาโนเมตรของคาร์บอนได้ปริมาณมาก ได้แก่ อัตราส่วนระหว่างขนาดของเส้นผ่าศูนย์กลางของแท่งเทียนต่อขนาดของเส้นผ่าศูนย์กลางของไส้เทียนเท่ากับ 0.5:2 ความยาวของไส้เทียนจากผิวด้านบนสุดของแท่งเทียนไข เท่ากับ 1.0 เซนติเมตร ตำแหน่งของเปลวไฟที่ถูกครอบกวนคือระหว่างบริเวณที่ 4 และ 5 ระยะความห่างของเส้นลวดที่ใช้ในการสานตัวครอบกวนเปลวไฟเท่ากับ 0.1 เซนติเมตร ชนิดของเส้นลวดที่ใช้ในการสานตัวครอบกวนเปลวไฟ คือ เส้นลวดนิโครม และลักษณะรูปร่างของตัวครอบกวนเปลวไฟคือรูปร่างสี่เหลี่ยม รูปร่างทรงกลมของอนุภาคระดับนาโนเมตรของคาร์บอนมีขนาด 20-100 นาโนเมตร ตรวจสอบโดยใช้กล้องจุลทรรศน์อิเล็กตรอนแบบส่องผ่าน กล้องจุลทรรศน์อิเล็กตรอนแบบส่องกราด และกล้องจุลทรรศน์แรงอะตอม พื้นที่ผิวของอนุภาคระดับนาโนเมตรของคาร์บอนตรวจสอบโดยใช้เทคนิคบีอีทีที่มีขนาด 95.05 ตารางเมตรต่อกรัม เอกซ์-เรย์ สเปกโทรสโกปี และรามานสเปกโทรสโกปี บอกถึงโครงสร้างของอนุภาคระดับนาโนเมตรของคาร์บอนเป็น โครงสร้างผสมกันของ โครงสร้างแกรไฟต์ แกรไฟต์ที่เรียงตัวไม่เป็นระเบียบ และ อัญฐาน พิกของอินฟราเรดเปกตราของอนุภาคระดับนาโนเมตรของคาร์บอนพบว่าไม่มีการสั่นแบบยืดของพันธะระหว่างคาร์บอนกับไฮโดรเจน แสดงว่าอนุภาคระดับนาโนเมตรของคาร์บอนที่สังเคราะห์ประกอบด้วยคาร์บอนที่มีความบริสุทธิ์ นอกจากนี้อนุภาคระดับนาโนเมตรของคาร์บอนสามารถนำไปประยุกต์ใช้ในการเป็นตัวดูดซับสารระเหยอินทรีย์ได้

สาขาวิชาปิโตรเคมีและวิทยาศาสตร์พอลิเมอร์  
ปีการศึกษา 2552

ลายมือชื่อนิสิต เขาวพา สารระจันทร  
ลายมือชื่อ อ.ที่ปริกษาวิทยานิพนธ์หลัก 



# # 5072435623 : MAJOR PETROCHEMISTRY AND POLYMER SCIENCE

KEYWORDS : CARBON NANOPARTICLES / PARAFFIN / FLAME COMBUSTION SYNTHESIS

YAOWAPA SARAJAN : SYNTHESIS AND CHARACTERIZATION OF CARBON NANOPARTICLES BY PARAFFIN COMBUSTION .

THESIS ADVISOR : ASSOC. PROF. SANONG EKGASIT, Ph.D., 78 pp.

In this study, carbon nanoparticles (CNPs) were synthesized by flame combustion of paraffin. The paraffin wax was shaped into candle and employed as carbon source. Various factors affecting CNPs synthesis were studied. All of these optimal factors can produce the highest yield of CNPs as follows: the ratio between diameter of candle wick and candle body was 0.5:2; the length of candle wick above the top surface of the candle body was 1.0 cm; the position of candle flame disturbance was carried out between the fourth and the fifth zones; the candle flame disturbance grid interval was 0.1 cm; the wire for the grid weaving was nichrome wire and the grid shape was square. The obtained spherical CNPs had particle size of 20-100 nm as observed via scanning electron microscopy (SEM), transmission electron microscopy (TEM), and atomic force microscopy (AFM). The surface area of CNPs determined by BET technique was 95.05 m<sup>2</sup>/g. X-ray diffraction (XRD) and Raman spectroscopy suggested that the synthesized CNPs are the combination of graphite, disorder graphite and amorphous structure. The infrared spectra of the CNPs suggested that there was no observable C-H stretching vibration in the synthesized particles. This indicated that the synthesized CNPs consist of pure carbon. Additionally, CNPs can be applied as the volatile organic compound adsorber.

Field of Study : Petrochemistry and  
Polymer Science.....

Academic Year : 2009.....

Student's Signature เชาวพา สารเจ้าพรวิ

Advisor's Signature ๑๐

## ACKNOWLEDGEMENTS

The author sincerely thanks my thesis advisor, Associate Professor Dr. Sanong Ekgasit for his advising suggestion, deeply discussion, understanding as well as patiently practices my technical skill during the whole research and encouragement to pass the problem and obstacle throughout this research.

The author would like to thank Associate Professor Dr. Sirirat Kokpol, Associate Professor Dr. Wimonrat Trakarnpruk, and Assistant Professor Dr. Toemsak Srihirin for usefully substantial suggestions as the thesis committee. Finally, the author would like to have the special thank to Associate Professor Chuchaat Thammacharoen who provided a great many useful insights.

The author would like to acknowledge Mr. Wonchalem Rungswang, and Associate Professor Dr. Suwabun Chirachanchai for the morphological characterization using transmission electron microscope, Miss Passimon Kongyou (forensic scientist) for the structural characterization by mean of Raman spectroscopy of Central Institute of Forensic Science (CIFS), Thailand, Miss Janthana Raruenrom (Forensic Toxicology and Chemistry Division) for the molecular characteristic characterization of the adsorbed volatile organic compound of the synthesized carbon nanoparticles (CNPs) by Gas Chromatography/Flame Ionization Detector (GC/FID), Mr. Taveesak Junduang for the candle body cutting apparatus, Mr. Vichit Palaprom for the candle flame disturbance weaving as a dome shape, Mr. Attapon Pongsuthipanich for encouragement in working and helpful all of things, National Center of Excellence for Petroleum, Petrochemicals and Advanced Materials (NCE-PPAM) and the Commission on Higher Education for partial financial support.

Whatever shortcomings in the thesis remain, they are the sole responsibility of the author.

Above all, The author wholeheartedly thanks my wonderful parents for their love, understanding, encouragement, and overwhelmingly support in my life throughout the course of education.

# CONTENTS

	Page
ABSTRACT (THAI).....	iv
ABSTRACT (ENGLISH).....	v
ACKNOWLEDGEMENTS.....	vi
CONTENTS.....	vii
LIST OF FIGURES.....	x
LIST OF TABLES.....	xiv
LIST OF ABBREVIATIONS.....	xv
LIST OF SYMBOLS.....	xvi
CHAPTER I INTRODUCTION.....	1
CHAPTER II THEORETICAL BACKGROUND.....	3
2.1 Paraffin wax.....	3
2.2 Candle flame.....	4
2.3 Carbon nanoparticles (CNPs).....	7
2.4 Flame combustion synthesis techniques.....	9
2.4.1 The premixed flames.....	9
2.4.2 The diffusion flames.....	9
2.5 Analytical instruments.....	10
2.5.1 Attenuated Total Reflection Fourier Transform Infrared (ATR FT-IR) Microspectroscopy.....	10
2.5.2 X-ray diffraction (XRD).....	11
2.5.3 Raman spectroscopy.....	12
2.5.4 Scanning electron microscope (SEM).....	13
2.5.5 Transmission electron microscope (TEM).....	14
2.5.6 Atomic force microscopy (AFM).....	15
2.5.7 N <sub>2</sub> adsorption/desorption analysis.....	16
2.5.8 Gas Chromatography/flame ionization detector (GC/FID).....	17

	Page
CHAPTER III EXPERIMENTAL SECTION.....	18
3.1 Materials.....	18
3.2 Experimental section.....	19
3.2.1 Candle casting from paraffin wax.....	19
3.2.2 Apparatus setting for CNPs synthesis.....	19
3.2.3 Preparation of the grid.....	20
3.2.4 The flame disturbance of candle.....	21
3.2.5 The adsorption testing of volatile organic compound by CNPs	22
3.2.5.1 CNPs pellet casting for adsorption of eucalyptus oil...	22
3.2.5.2 CNPs pellet casting for adsorption of diesel oil.....	23
3.3 Characterization of CNPs.....	24
3.3.1 The molecular information and crystal structure	
characterization.....	24
3.3.1.1 ATR FT-IR microspectroscopy.....	24
3.3.1.2 X-ray diffraction (XRD).....	25
3.3.1.3 Raman spectroscopy.....	25
3.3.1.4 Gas Chromatography/Flame Ionization Detector	
(GC/FID).....	25
3.3.2 Morphology analysis/Imaging technique.....	26
3.3.2.1 Scanning electron microscope (SEM).....	26
3.3.2.2 Transmission electron microscope (TEM).....	26
3.3.2.3 Atomic force microscopy (AFM).....	26
3.3.3 Surface area analysis.....	27
3.3.3.1 N <sub>2</sub> adsorption/desorption analysis.....	27
CHAPTER IV RESULTS AND DISCUSSION.....	28
4.1 The diameter of candle wick.....	28
4.2 The ratio of diameter of candle wick and candle body.....	31



	Page
4.3 The length of candle wick above the top surface of candle body.....	34
4.4 The candle flame disturbance of each flame zone.....	37
4.5 The grid interval of candle flame disturbance.....	44
4.6 The effect of material of grid on candle flame disturbance.....	46
4.7 The grid shape in the candle flame disturbance.....	47
4.8 The characterizations of CNPs.....	48
4.8.1 The molecular information and crystal structure.....	48
4.8.1.1 ATR FT-IR microspectroscopy.....	48
4.8.1.2 X-ray diffraction (XRD).....	49
4.8.1.3 Raman spectroscopy.....	50
4.8.2 Morphology analysis/Imaging technique.....	52
4.8.2.1 Scanning electron microscopy (SEM).....	52
4.8.2.2 Transmission electron microscopy (TEM).....	53
4.8.2.3 Atomic force microscopy (AFM).....	55
4.8.3 Surface area analysis.....	56
4.8.3.1 N <sub>2</sub> adsorption/desorption analysis.....	56
4.8.4 The volatile organic compound adsorption of CNPs.....	58
4.8.4.1 Adsorption of eucalyptus oil by CNPs pellet.....	59
4.8.4.2 Adsorption of diesel oil by CNPs pellet.....	60
CHAPTER V CONCLUSIONS.....	65
REFERENCES.....	66
APPENDIX.....	70
VITAE.....	78

## LIST OF FIGURES

Figure		Page
2.1	The candle flame zones.....	6
2.2	Schematic mechanism of the formation of soot particles.....	6
2.3	The structure of carbon spheres in three categories: (A) Carbon ions, (B) Carbon spheres, and (C) Carbon beads.....	8
2.4	Schematic diagram of the flame synthesis process.....	10
2.5	ATR FT-IR microscope: (A) Continuum <sup>TM</sup> infrared microscope attached to the Nicolet 6700 FT-IR spectrometer, (B) the slide-on Ge $\mu$ IRE is fixed on the position of slide-on housing on the infrared objective, and (C) Homemade slide-on Ge $\mu$ IRE.....	11
2.6	Diffraction of X-ray by regular planes of atom.....	12
2.7	Quantum representation of energy interchange involved in the Raman effect.....	13
2.8	Schematic diagram of scanning electron microscope (SEM).....	14
2.9	Schematic diagram of transmission electron microscope (TEM).....	15
2.10	Schematic diagram of real micro-cantilever and components of AFM.....	16
3.1	The apparatus for CNPs synthesis.....	19
3.2	The chess square grid with the grid interval of (A) 0.1 cm, (B) 0.5 cm, and (C) 1.0 cm.....	20
3.3	The various wire type for grid weaving (A) copper wire, (B) iron wire, and (C) nichrome wire.....	20
3.4	The various grid shapes (A) square and (B) dome (the height of 6.0 cm. and the diameter of 3.0 cm).....	21

Figure	Page	
3.5	The flame combustion of candle wax: (A) the flame disturbance with the grid, (B) the candle flame zone, (C) CNPs on aluminium plate, (D) CNPs on the grid, and (E) CNPs powder.....	21
3.6	CNPs pellet with adsorbed–volatile compound.....	23
4.1	ATR spectra of paraffin wax and CNPs from the synthesis with candle wick of each diameters: (A) paraffin wax, (B) the diameter of 0.15 cm, and (C) the diameter of 0.5 cm .....	31
4.2	ATR spectra of CNPs from the synthesis with diameter ratio of candle wick to candle body variable (cm:cm) (A) 0.5:2 (B) 0.5:4 (C) 0.5:6, and (D) 0.5:8.....	33
4.3	The combustion of various lengths of candle wick: (A) 0.5 cm, (B) 1.0 cm, (C) 1.5 cm, (D) 2.0 cm, (E) 2.5 cm, and (F) 3.0 cm.....	35
4.4	The disturbed candle flame between the second and the third zone (A) candle flame which was not disturbed, (B) The inserted glass slide at the position of the candle flame disturbance, (C) The candle flame disturbance between the second and the third zone by glass slide (D) CNPs film on glass slide after the candle flame disturbance, and (E) The processed image of CNPs film.....	37
4.5	ATR spectra of various regions of CNPs film on glass slide by the candle flame disturbance between the second and the third zone..	39
4.6	The disturbed candle flame between the third and the fourth zone. (A) The candle flame which was not disturbed, (B) The inserted glass slide at the position of the candle flame disturbance, (C) The candle flame disturbance between the third and the fourth zone by glass slide (D) CNPs film on glass slide after the candle flame disturbance, and (E) The processed image of CNPs film.....	40

Figure	Page	
4.7	ATR spectra of various regions of CNPs film on glass slide by the candle flame disturbance between the third and the fourth zone.....	41
4.8	The disturbed candle flame between the fourth and the fifth zone. (A) The candle flame which was not disturbed, (B) The inserted glass slide at the position of the candle flame disturbance, (C) The candle flame disturbance between the fourth and the fifth zone by glass slide (D) CNPs film on glass slide after the candle flame disturbance and (E) The processed image of CNPs film.....	42
4.9	ATR spectra of CNPs films along its diameter on glass slide by the candle flame disturbance between the fourth and the fifth zone.....	43
4.10	ATR spectrum of the synthesized CNPs.....	49
4.11	XRD pattern of CNPs with (A) the synthesized CNPs and (B) CNPs (Yi, Z. et. al. (2007)).....	50
4.12	Raman spectra of CNPs with (A) original peaks and (B) the curve fitted peaks.....	52
4.13	SEM images of CNPs: (A) CNPs thin film on aluminium plate, (B) CNPs thick film on aluminium plate, and (C) CNPs powder.....	53
4.14	TEM images of CNPs (A)–(C) chain like structure of CNPs and (D)–(F) CNPs after ultrasonic in ethanol for 1 hour.....	54
4.15	Histogram of the particle size of the synthesized CNPs by flame combustion technique.....	54
4.16	AFM image of CNPs after ultrasonicated in ethanol ((A1) and (A2)), CNPs after exposing on cover glass directly to the soot ((B1) and (B2)), and CNPs after exposing the thin ethanol film coated on glass slide directly to the soot ((C1) and (C2)).....	56
4.17	The volatile organic compound adsorber: (A) CNPs pellet and (B) the charcoal strip (commercial product).....	59
4.18	ATR spectra of (A) CNPs pellet, (B) eucalyptus oil, and (C) CNPs pellet with adsorbed-eucalyptus aroma.....	60

Figure		Page
4.19	Feature of CNPs pellet: (A) condensed CNPs pellet with tolerable durability and (B) brittle CNPs pellet.....	61
4.20	GC peaks of (A) charcoal strip (commercial product), (B) diesel oil, and (C) charcoal strip with adsorbed–diesel oil.....	63
4.21	GC peaks of (A) CNPs pellet, (B) diesel oil, and (C) CNPs pellet with adsorbed–diesel oil.....	64



ศูนย์วิทยทรัพยากร  
จุฬาลงกรณ์มหาวิทยาลัย



## LIST OF TABLES

Table		Page
2.1	The properties of paraffin candle wax.....	3
3.1	The condition of CNPs pellet casting for adsorption of eucalyptus oil.....	22
3.2	The conditions of CNPs pellet casting with Teflon powder as binder.....	23
3.3	The conditions of CNPs pellet casting with paper pulp as binder.....	24
4.1	Comparison of the diameter of candle wick in synthesis of CNPs.....	29
4.2	The candle flames of each diameter ratio of candle wick and candle body in CNPs synthesis .....	32
4.3	The candle flame disturbance by various grid intervals and yield of CNPs (%)......	45
4.4	Thermal conductivity ( $Wm^{-1}K^{-1}$ ) and yield of CNPs (%) of the various wire types of the grid weaving in candle flame disturbance...	47
4.5	Yield of CNPs (%) on disturbance grid.....	48
4.6	The specific surface area comparisons of various particle size of CNPs.....	58
4.7	The theoretical surface area of the synthesized CNPs.....	58
4.8	The result of CNPs pellet casting with various condition.....	59
4.9	The result of CNPs pellet casting with Teflon powder as binder.....	61
4.10	The result of CNPs pellet casting with paper pulp as binder.....	61

## LIST OF ABBREVIATIONS

CNTs	: Carbon nanotubes
CNFs	: Carbon nanofibers
CNPs	: Carbon nanoparticles
CVD	: Chemical Vapor Deposition
XRD	: X-ray diffraction
SEM	: Scanning Electron Microscope
TEM	: Transmission Electron Microscope
AFM	: Atomic Force Microscopy
PZT	: Piezoelectric
ATR	: Attenuated total reflection
FT-IR	: Fourier transform infrared
GC/FID	: Gas Chromatography/Flame Ionization Detector (GC/FID).
kg	: Kilogram
kmol	: Kilo mole
kPa	: Kilo Pascal
nm	: Nanometer ( $10^{-9}$ m)
cm	: Centimeter ( $10^{-2}$ m)
mg	: Milligram ( $10^{-3}$ g)
L	: Liter
mL	: Milliliter ( $10^{-3}$ L)
mA	: Milliamp
keV	: Kilo electron volt
IRE	: Internal reflection element
kV	: Kilovolt ( $10^3$ V)
M	: Molar
MCT	: Mercury-cadmium-telluride
v	: Volume
wt	: Weight
w	: Weak band
ZnSe	: Zinc selenide

## LIST OF SYMBOLS

$^{\circ}\text{C}$	: Degree Celsius
$\text{m}^3$	: Cubic meter
$n$	: Order of reflection
$\lambda$	: The X-ray wavelength
$d$	: The inter planar spacing
$\theta$	: The diffraction angle
$W$	: The weight of nitrogen adsorbed at a given $P/P_0$
$W_m$	: The weight of gas to give monolayer coverage
$C$	: A constant related to the heat of adsorption



ศูนย์วิทยทรัพยากร  
จุฬาลงกรณ์มหาวิทยาลัย

# CHAPTER I

## INTRODUCTION

Carbon-based nanomaterials such as carbon nanotubes (CNTs), buckminsterfullerenes, carbon nanofibers (CNFs), and carbon nanoparticles (CNPs) have very small size (in nanometer) [1]. CNPs have been attracted a lot of interests, and are currently an area of intense scientific research, due to a wide variety of potential applications in biocompatible materials, biosensing, conductive materials, drug delivery, filler, electrical component, adsorber, and much more [2]. CNPs can be synthesized by various techniques such as pulsed laser ablation (KrF excimer laser) in argon [3], chemical vapor deposition (CVD) by methane ( $\text{CH}_4$ ) as carbon source [4], arc discharge in liquid nitrogen [5], direct pyrolysis of hydrocarbons, including styrene, toluene, benzene, hexane, cyclohexane and ethane, in the absence of catalyst [6] and flame synthesis which used acetylene as a carbon source. CNPs were deposited on porous silicon plate by electrochemistry [7]. All of these techniques required complex and expensive instruments. Obviously, the flame combustion synthesis technique with hydrocarbon compound as a carbon source such as, acetylene gas ( $\text{C}_2\text{H}_2$ ), propane ( $\text{C}_3\text{H}_8$ ) etc, is simple and inexpensive. Soot or CNPs is formed after disturbing the system, in which there is locally insufficient oxygen. With advantages of this technique, the particles that are highly pure, small sizes, and have relatively narrow size distribution can be produced. In this research, CNPs were synthesized by flame combustion of candle wax which was simple technique and low cost operation. Furthermore, the candle wax made from paraffin was the residues from petrochemical industry. This makes the value-added of residue from petrochemical industry. In addition, CNPs have lots of promising applications.

### 1.1 The objectives

To synthesize CNPs by flame combustion technique, and to characterize the molecular characteristics of CNPs by means of ATR FT-IR microspectroscopy, X-ray diffraction (XRD), Raman spectroscopy, scanning electron microscopy (SEM), transmission electron microscopy (TEM), atomic force microscopy (AFM), and

N<sub>2</sub> adsorption/desorption analysis. In addition, CNPs are also tested as volatile organic compound adsorber.

## 1.2 The scopes of this research

1. Synthesizing CNPs by flame combustion technique.
2. Obtaining the molecular information of CNPs by means of ATR FT-IR microspectroscopy, X - ray diffraction (XRD), and Raman spectroscopy.
3. Characterizing particles size and morphology of CNPs by means of scanning electron microscopy (SEM), transmission electron microscopy (TEM), and atomic force microscopy (AFM).
4. Evaluating the surface area of CNPs by N<sub>2</sub> adsorption/desorption analysis.
5. Applying the synthesized CNPs as an adsorber of volatile organic compound, which were investigated by ATR FT-IR microspectroscopy and gas chromatography/flame ionization detector (GC/FID).

## 1.3 Expected benefits

CNPs are extremely small (approximately less than 100 nm), highly pure, and have high surface area. It has high potential applications for volatile organic compound adsorber.

ศูนย์วิทยทรัพยากร  
จุฬาลงกรณ์มหาวิทยาลัย



## CHAPTER II

### THEORETICAL BACKGROUND

#### 2.1 Paraffin wax

The paraffin wax was derived from petrochemical industry. These waxes are residues extracted when dewaxing crude oils [8]. The most general type of paraffin wax used in solid fuel or the candle making process [9]. The paraffin wax is the primary component of a candle, which is a composite material made of a mixture of straight-chain hydrocarbon molecules. The molecular formula of paraffin is  $C_nH_{2n+2}$ , which the value of  $n$  ranges from 19 to 36 and the average value are 23-25. The molecular weight (average) is 350-420 kg/kmol. The characteristics of a particular paraffin wax are commonly defined by its physical properties. These properties include melting point, melted wax temperature (average, around base of wick), flash point, maximum flame temperature and others listed in Table 2.1.

Table 2.1 The properties of paraffin candle wax [9].

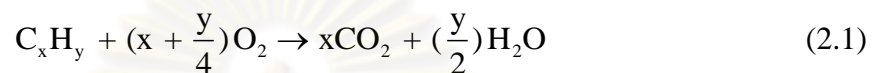
Properties of paraffin wax	Value
Carbon number, range ( $C_nH_{2n+2}$ )	19-36
Carbon number, average ( $C_nH_{2n+2}$ )	23-25
Molecular weight (average)	350-420 kg/kmol
Melting point	48-68 °C
Melted wax temperature (average, around base of wick)	82-85 °C
Maximum flame temperature	1400 °C
Flash point	66-69 °C
Fire point	204-271 °C
Boiling point	238-263 °C
Density (at room temperature)	865-913 kg/m <sup>3</sup>
Vapor pressure (at 100 °C)	2.67 kPa

## 2.2 Candle flame

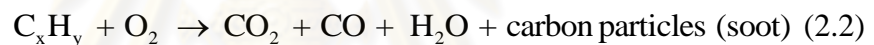
The body of a candle is a solid fuel source that is usually paraffin wax. The wick runs through the center of the candle body from the bottom, extending out of the top. A wick acts as a fuel pump when the candle is combusted. A wick is commonly made of cotton fibers that have been braided together as shown in Figure 2.1A. The candle combustion will occur from fire setting on the wick and heat from the flame travels rapidly toward the candle body. It is instantly melted to liquid wax which is pulled up the wick by capillary attraction or the attractive molecular forces between the wax molecules and the wick molecules pull the wax upward. The liquid wax creeps to near the top of the wick. It is vaporized and released hydrocarbon or carbon molecule. The cycle of the candle combustion repeats itself until the wick is exhausted. It will lack fuel for the flame that may die out [10-11]. The interesting point of the candle is the flame. The position of the combustion can be classified into five zones as shown in the processed image of the candle flame (Figure 2.1B). From the processed image of the exact candle flame, reaction zones can be classified into five zones as follows [12]:

- Zone 1 (Non-Luminous Zone): The wax is evaporated. There is insufficient oxygen for fuel to combust. (Temperature ~ 600 °C)
- Zone 2 (Blue Zone): There is a surplus of oxygen starting and the flame of combustion begins. It has blue color. (Temperature ~ 800 °C)
- Zone 3 (Dark Zone): The cracking of the wax begins because there is insufficient oxygen for combustion. Therefore, it will create minute carbon particles. (Temperature ~ 1000 °C)
- Zone 4 (Luminous Zone): There is still insufficient oxygen for complete combustion. Therefore, the continuous cracking of this zone will produce a lot of carbon particles. This area is bright yellow. (Temperature ~ 1200 °C)
- Zone 5 (Veil): There is a surplus of oxygen in this non-luminous zone. The carbon particles react with oxygen to form carbon dioxide (CO<sub>2</sub>). The hydrogen atoms react with free oxygen to form water (H<sub>2</sub>O). The complete combustion occurs in this zone. (Temperature ~ 1400 °C)

The fundamentals of combustion can be termed as the process of establishing self-sustained fire using fuel and oxidizer in a controlled manner. The overall chemical process is exothermic in nature, which liberates enough heat to self-sustaining combustion process. The combustion can be divided to the complete combustion and the incomplete combustion. In the complete combustion, when the reactant (hydrocarbon compound is usually used as fuel) will burn in sufficient oxygen. The production will gain only yield of carbon dioxide (CO<sub>2</sub>) and water (H<sub>2</sub>O) as follows [13]:



The incomplete combustion occurs when there is insufficient oxygen. The hydrocarbon compound burns in air. Therefore, the production will gain yield of carbon dioxide (CO<sub>2</sub>), water (H<sub>2</sub>O), carbon monoxide (CO), carbon particles (soot) and various other compound which react with hydrogen and oxygen as follows [13]:



The carbon particles (soot) formation occurs from incomplete combustion. The mechanism of the reacting species is extremely complex, and many pathways lead to the polycyclic structures which are the building blocks of the soot particles. One of the main pathways is the following. Certain molecules are pyrolyzed into small unsaturated molecules where the main constituent is ethyne. The ethyne polymerizes to polyethyne. Eventually, polycyclic structures are formed by ring closure. These polycyclic structures are called platelets or small graphitelike sheets that could be seen as the primary building blocks of the soot particle. The platelets stack together to form crystallites, which subsequently stack together to form turbostratic particles, as shown in Figure 2.2. The size of the particles increases due to particle coagulation and surface growth instigated by the addition of precursor gas-phase molecules. The surface growth fills the space between the coagulated particles. The coagulated particles remain spherical. Ishiguro et al. [14] showed that surface growth platelets do not orient themselves in a turbostratic manner, instead they are oriented perpendicular to the radius of the particle, which gives the soot particles a rigid outer shell, which is thermodynamically more stable than the turbostratic inner

core. When surface growth stops, the growth of the spherical particles stops. These particles are then called primary soot particles. Those primary soot particles continue to coagulate and form chainlike aggregates, the so-called “secondary soot particles” [15].

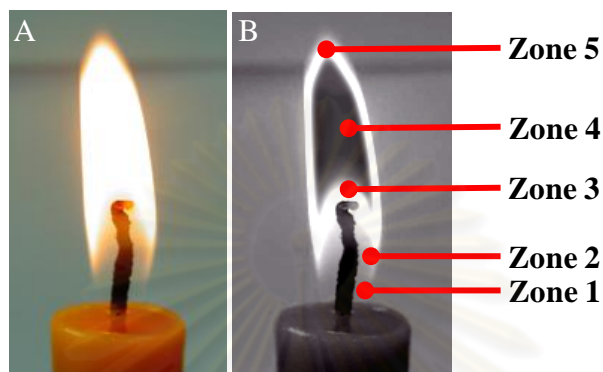


Figure 2.1 The candle flame zones.

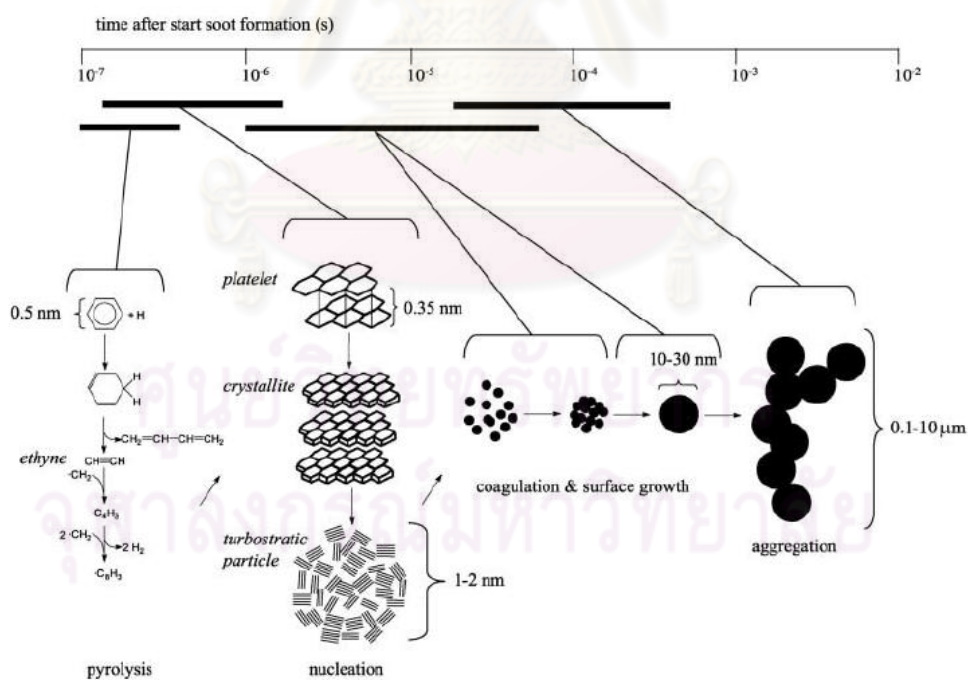


Figure 2.2 Schematic mechanism of the formation of soot particles [15].

### 2.3 Carbon nanoparticles (CNPs)

Carbon-based nanomaterials, which consist of carbon nanotubes (CNTs), fullerenes, carbon nanofibers (CNFs) and carbon nanoparticles (CNPs), have promising applications in nanotechnology. Among these, CNPs have gained much more attention due to their prospective characteristics. The discovery of CNPs or spherical carbon structure are attracting extensive attention due to their excellent properties and potential application as biocompatible materials, biosensing, conductive materials, drug delivery, filler, electrical component, adsorber etc.

Inagaki, M. defines a classification of these spherical carbon structures as follows (with respect to their nanometric texture): concentric, radial and random arrangements of the carbon layer [16]. CNPs can also be classified with respect to the size of carbon spheres in three categories as follows [17]:

- (i) The well graphitized onion like structure which typically have diameters of 2-20 nm (Figure 2.3A).
- (ii) The carbon nanospheres which demonstrate less graphitized structures and have diameters between 50 nm and 1  $\mu\text{m}$  (Figure 2.3B).
- (iii) The carbon beads have diameters of one to several microns (Figure 2.3C).

From literature reviews of the CNPs, there are several methods for synthesizing CNPs as follows:

Chen G.X. et. al. (2004) [3] synthesized CNPs by pulsed laser ablation (KrF excimer laser) in argon gas. The pressure was held at 0.01–1 Torr. The graphite was used as a carbon source. CNPs had the particles size 7-13 nm which depend on increasing of a pressure. They found that, from SEM images as observed via morphologies of CNPs having highly roughed and transferred to a cauliflower-like structure at 0.60 Torr and a floccus-like structure at 1.0 Torr. CNPs were suggested highly disordered and amorphous structure by Raman spectroscopy and X-ray diffraction (XRD).

Yu J. et. al. (2002) [4] has used Chemical Vapor Deposition method for CNPs synthesis by methane ( $\text{CH}_4$ ) gas as a carbon source. The iron film that had the



thickness 200 nm was used as catalysts for carbon atom cracking at pressure 4000 Pa, temperature 670 °C and were held 15 minutes. They found that this method had grown the CNPs and CNTs which had particles size from 10 nm to more than 200 nm and wide size distribution as observed via SEM image. There was polycrystalline graphite structure which analyzed by Raman spectroscopy

Charinpanitkul T. et. al. (2008) [5] synthesized CNPs by arc discharge in liquid nitrogen. Iron and graphite electrodes (cathode electrode) were compared. A current was varied in a range of 50–250 Ampere (A.). They found that the current about 100 A were applied into iron electrode or graphite electrode. Carbon nanocapsules (a particles size 50–400 nm) were grown from iron electrode and multiwalled carbon nanotubes (MW-CNTs) (diameter 8–25 nm and length 150-250 nm) were grown from graphite electrode. However, this method will get a few CNPs when current applying was increased.

Quercia L. et. al. (2004) [18] produced CNPs by flame synthesis which used acetylene as a carbon source. CNPs were deposited on porous silicon plate by electrochemistry. CNPs had a particles size 5-20 nm as observed via SEM. XRD technique revealed poly-fullerenes structure of CNPs. The infrared spectra of CNPs suggested that there was no observable C-H and C-O peaks as observed via FT-IR spectroscopy. And then CNPs were mixed with poly(methyl-methacrylate) in order to apply as sensor for adsorbed volatile compound (acetone). They found that CNPs had potential in adsorbed volatile compound more than that of general carbon.

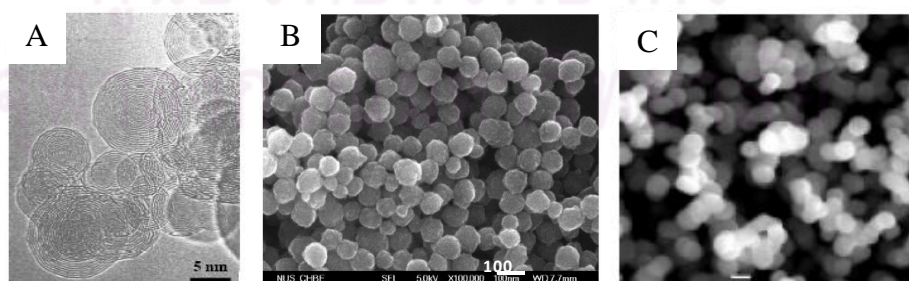


Figure 2.3 The structure of carbon spheres in three categories: (A) Carbon onions [19], (B) Carbon spheres [20], and (C) Carbon beads [21].

## 2.4 Flame combustion synthesis techniques

Flame combustion synthesis (Figure 2.4) is one of the promising mass production techniques for CNPs. The method is cost effective and provides a high production rate. The apparatus set up is a simple and low cost. A typical flame aerosol set-up consists of a precursor unit (evaporator), a burner accompanied by a gas delivery system and a filter unit to collect the product particles. Various flame configurations are used for the manufacture of CNPs as follows:

### 2.4.1 The premixed flames

The combustion gases are mixed before they enter the reaction flame zone. They are hydrocarbon compound such as, acetylene gas ( $C_2H_2$ ), propane ( $C_3H_8$ ), methane ( $CH_4$ ) etc. depending on the gas flow rates and burner geometry, flame either laminar or turbulent. In industry turbulent co-flow reactor are usually used, since large quantities of particles are desired [13].

### 2.4.2 The diffusion flames

The fuel and oxidizer are unmixed even up to flame surface. In other words, fuel and oxidizer are mixed and burnt instantaneously at the flame surface itself. Some of the examples of diffusion flame-based combustion system are wood stoves, coal burner, industrial furnaces, a candle flame etc. As a result, the burning rate is dictated by the rate which fuel and oxidizer can reach together at the flame surface in proper proportions [13].

This method used various flame types in synthesis. Hydrocarbon compound was used as the fuel or a carbon source in CNPs synthesis. Soot (black smoke) or carbon particles are formed after a flame disturbing, which there is locally insufficient oxygen or incomplete combustion, combined with the interaction of catalyst, and created an appropriate environment for the formation of CNPs. Synthesis from the premixed flames can produce CNTs. However, synthesis from the diffusion flames can produce CNPs. With advantages of flame combustion technique, the

particles with highly pure, small sizes and relatively narrow size distribution can be produced [22].

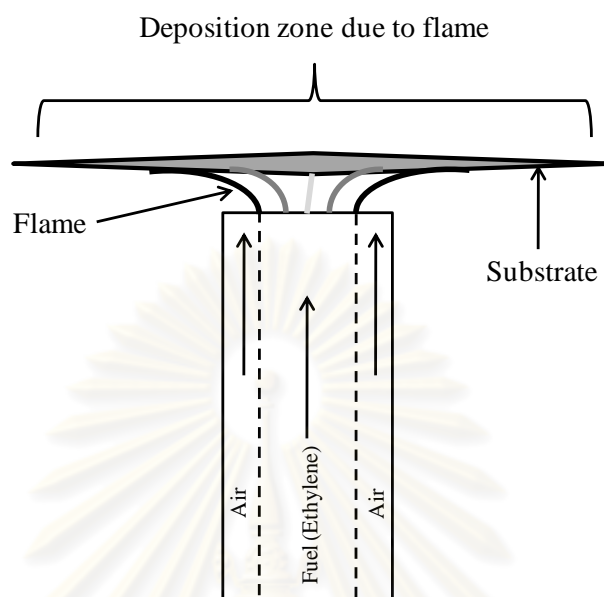


Figure 2.4 Schematic diagram of the flame combustion synthesis process

## 2.5 Analytical instruments

### 2.5.1 Attenuated Total Reflection Fourier Transform Infrared (ATR FT-IR) Microspectroscopy

Attenuated total reflection Fourier transform infrared spectroscopy is used for analysis of surface of materials and is a non-destructive technique. It is a method of internal reflection, which requires a medium called internal reflection element (IRE) or the *ATR crystal*. The infrared radiation is directed into IRE, which has high refractive index with an angle that total internal reflections occur inside IRE. The light exits IRE and passes through the spectrometer to the detector. At each reflection, a part of the light called the *evanescent wave* passes IRE interface and interacts with a sample placed in close contact with IRE. The infrared spectrum may be collected. The surface of a sample is pressed into optical contact of IRE such as zinc selenide (ZnSe), germanium (Ge), and diamond. The materials of IRE have an effect on the ATR measurement because materials of different refractive index affect the depth of penetration and the occurrence of anomalous dispersion [23].

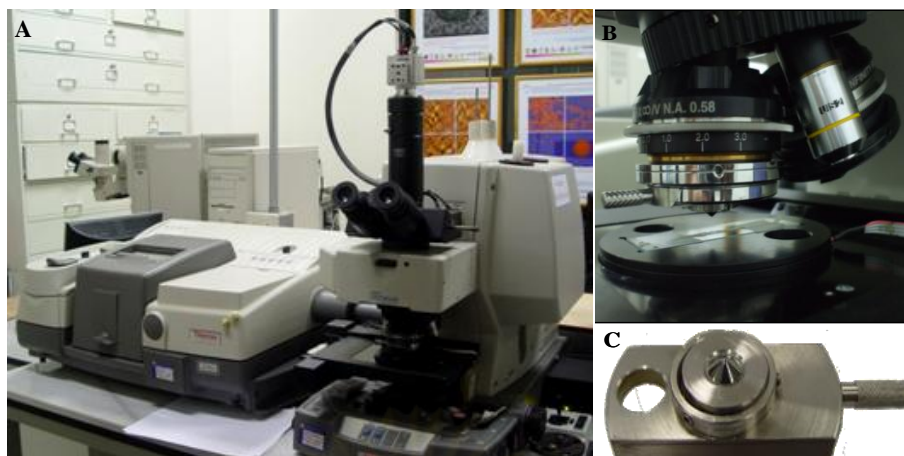


Figure 2.5 ATR FT-IR microspectroscopy: (A) Continuum™ infrared microscope attached to the Nicolet 6700 FT-IR spectrometer, (B) the slide-on Ge  $\mu$ IRE is fixed on the position of slide-on housing on the infrared objective, and (C) Homemade slide-on Ge  $\mu$ IRE.

### 2.5.2 X-ray diffraction (XRD)

XRD is the instrumental technique for characterization of crystalline structure materials. When X-ray radiation is directed on sample, it is scattered by electrons present in the sample. This scattering results in maxima and minima in the diffracted intensity. The signal maxima follow Bragg's law equation [24]:

$$n\lambda = 2d\sin\theta \quad (2.1)$$

where,  $n$  = order of reflection

$\lambda$  = the X-ray wavelength

$d$  = the inter planar spacing

$\theta$  = the diffraction angle

Figure 2.6 shows the diffraction of X-ray by regular planes of atom. Each lattice  $d$ -spacing, Bragg's law predicts a maximum at a characteristic diffraction angle ( $\theta$ ). During XRD measurement the angles of incidence and detection are scanned. When the intensity of detected X-ray is plotted as a function of angle ( $\theta$ ) an X-ray diffraction pattern is obtained, which is the sample characteristic. The usual information depth of XRD measurement ranges from a few micrometers to

hundred micrometers, depending on the density of the sample. Using a very small, fixed incidence angle of the X-rays (so-called grazing incidence measurement) thin layers of only a few nanometers can be investigated as well.

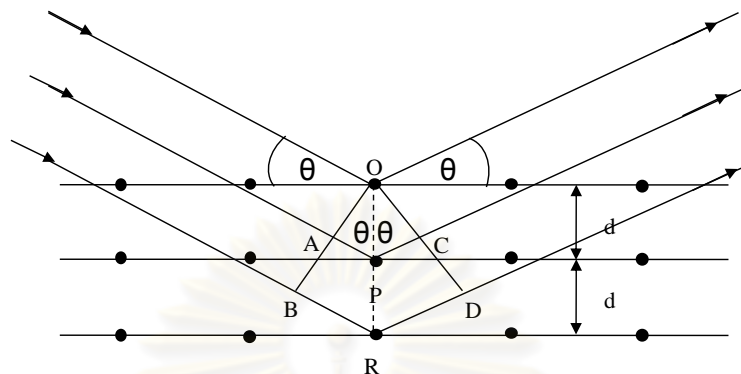


Figure 2.6 Diffraction of X-ray by regular planes of atom.

### 2.5.3 Raman spectroscopy

Raman spectroscopy is used for analysis of the structure of organic, inorganic and biological substances. The advantage of this technique is that the water does not interfere the Raman spectrum. The theory of Raman spectroscopy is defined that a photon is scattered by the molecular system. Most photons are elastically scattered, a process which is called Rayleigh scattering. In Rayleigh scattering, the emitted photon has the same wavelength as the absorbing photon. Raman spectroscopy is based on the Raman effect which is the inelastic scattering of photons by molecules. The Raman effect comprises a very small fraction, about 1 in  $10^7$ , of the incident photons. In Raman scattering, the energies of the incident and scattered photons are different. A simplified energy diagram is shown in Figure 2.7.

The energy of the scattered radiation is less than the incident radiation for the Stokes line. The energy of the scattered radiation is greater than the incident radiation for the anti-Stokes line. The energy increases or decreases from the excitation is related to the vibrational energy spacing in the ground electronic state of the molecule. Therefore, the wavenumber of the Stokes and anti-Stokes lines are the direct measurement of the vibrational energies of the molecule [25].



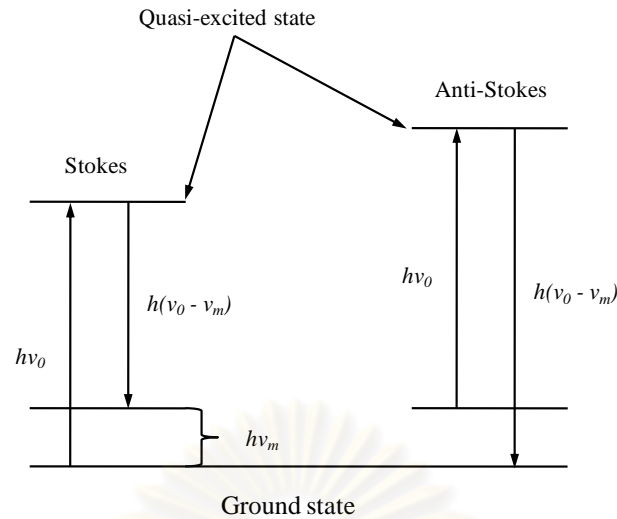


Figure 2.7 Quantum representation of energy interchange involved in the Raman effect.

#### 2.5.4 Scanning electron microscope (SEM)

SEM is widely used to characterize the information about surfaces of solid substrate. The conductive sample are easiest to study because the unimpeded flow of electrons to ground minimizes artifacts associated with the buildup of charge. For obtaining SEM image of non-conducting samples, it will involve the coating on the surface of the sample with a thin metallic film produced by sputtering or vacuum evaporation before surface characterization. In obtaining an electron microscopic image, the surface of sample is swept in a raster pattern with a finely focused beam of electrons. A raster is a scanning pattern that used in a cathode-ray tube, in which an electron beam is swept across a surface in a straight line, returned to its starting position, and shifted downward by a standard increment. This process is repeated until a desired area of the surface has been scanned. Schematic diagram of SEM was shown in Figure 2.8 [25].

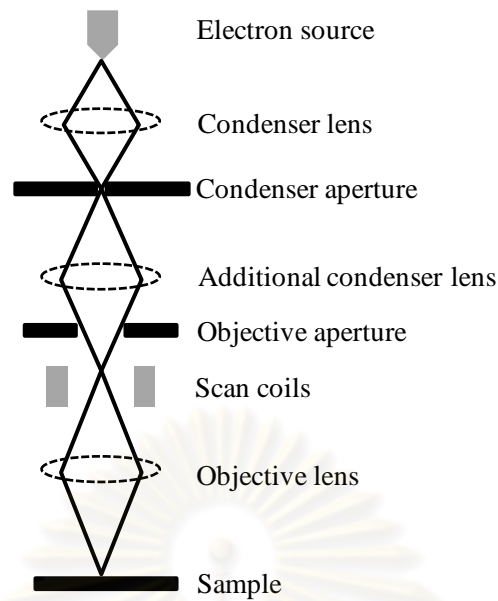


Figure 2.8 Schematic diagram of scanning electron microscope (SEM).

#### 2.5.5 Transmission electron microscope (TEM)

TEM is extensively used for studying the morphology size and size distribution of particles. TEM associates a beam of accelerated electron with energy of 50-200 keV and emitted by a cathode in vacuum. These electrons are deflected in small angles by atoms in sample and transmitted through thin sample. Then, these electrons are magnified by magnetic lenses and hitting a fluorescent screen generating the bright field image. Transmission electron microscope was shown in Figure 2.9. The electron interaction beam with atoms in the samples is the diffraction or absorption of electron beam. The images from electron microscopes indicate the structure of a sample which can be used for size determining, and characterizing morphology of nanoparticles [26].

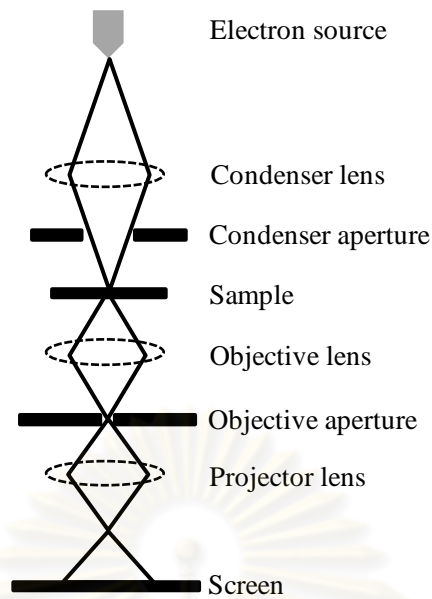


Figure 2.9 Schematic diagram of transmission electron microscope (TEM).

#### 2.5.6 Atomic force microscopy (AFM)

The atomic force microscope (AFM) has evolved into the instrumental technique for characterization of morphology of nanomaterial. A typical AFM system (Figure 2.10) consists of a micro-machined cantilever probe and a sharp tip mounted to a Piezoelectric (PZT) actuator and a position-sensitive photo detector for receiving a laser beam reflected off the end-point of the beam to provide cantilever deflection feedback. The fundamental of AFM operation is that the tip is scanned on the surface of the sample, and moves up and down with the contour of the surface, the laser beam deflected from the cantilever provides measurements of difference in light intensities between the upper and lower photo detectors. Feedback from the photodiode different signal through software control from the computer, enables the tip to maintain either a constant force or constant height deviation. In constant height mode, the deflection force on the sample is recorded [27].

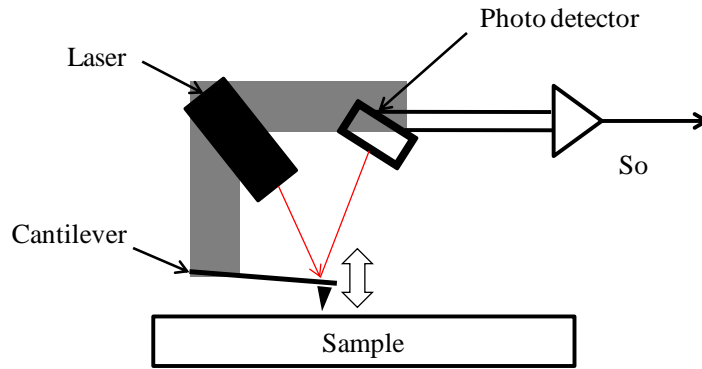


Figure 2.10 Schematic diagram of real micro-cantilever and components of AFM.

### 2.5.7 N<sub>2</sub> adsorption/desorption analysis

N<sub>2</sub> adsorption/desorption analysis is used to determine the physical properties of mesoporous molecular sieves such as the surface area, pore volume, pore diameter and pore-size distribution of solid catalysts. The Brunauer, Emmett, and Teller (BET) method [28] is generally used to measure total surface area.

$$\frac{1}{W[(P_0/P)-1]} = \frac{1}{W_m C} + \frac{C-1}{W_m C} (P/P_0) \quad (2.2)$$

where,

W = the weight of nitrogen adsorbed at a given P/P<sub>0</sub> (ratio between equilibrium pressure of adsorbates (P) and saturation pressure of adsorbates at temperature of adsorption (P<sub>0</sub>))

W<sub>m</sub> = the weight of gas to give monolayer coverage

C = a constant that is related to the heat of adsorption

A linear relationship between 1/W[(P/P<sub>0</sub>)-1] and P/P<sub>0</sub> is required to obtain the quantity of nitrogen adsorbed. This linear portion of the curve is restricted to a limited portion of isotherm, generally between 0.05-0.30. The slope and intercept are used to determine the quantity of nitrogen adsorbed in the monolayer, then the surface area is calculated. For a single point method, the intercept is taken as zero or a small positive value, and the slope from the BET plot is used to calculate the surface area. The reported surface area depends upon the method used, as well as the partial pressures in which the data are collected.

### 2.5.8 Gas Chromatography/flame ionization detector (GC/FID)

GC/FID is a method of separating mixtures of volatile compounds into their components which use the flame ionization as detector. It enables us to separate trace impurities or major fractions from each other. Based on the time required for separation, it can obtain considerable information on the identity of each component.

The flame ionization detector, FID, works by directing the gas phase output from the column to be mixed with hydrogen and air, and ignited. Organic compounds burning in the flame produce ions and electrons which can conduct electricity through the flame. A large electrical potential is applied at the burner tip, and a collector electrode is located above the flame. The current resulting from the pyrolysis of any organic compounds is measured. The FID is a useful general detector for the analysis of organic compounds; it has high sensitivity, a large linear response range, and low noise. It is also robust and easy to use, but unfortunately, it destroys the sample [24].

## CHAPTER III

### EXPERIMENTAL SECTION

Carbon nanoparticles (CNPs) were synthesized by flame combustion of candle wax. The characterizations of them were divided into three parts: (i) molecular information and crystal structure characterization, (ii) morphology analysis, and (iii) surface area analysis. To obtain the molecular information, ATR FT-IR microspectroscopy and Raman spectroscopy were carried out. Crystal structure determination was performed by X-ray diffraction (XRD). Scanning electron microscopy (SEM), transmission electron microscopy (TEM), and atomic force microscopy (AFM) were performed to estimate the particles size and morphology of CNPs. Surface area analysis by N<sub>2</sub> adsorption/desorption technique was employed to investigate the surface area of CNPs. The adsorption property of the synthesized CNPs was investigated by ATR FT-IR microspectroscopy and gas chromatography/flame ionization detector (GC/FID).

#### 3.1 Materials

1. Pure paraffin wax
2. Candle wick made of 100% cotton (diameter of 0.50 and 0.15 cm)
3. Aluminium plate
4. Stainless steel cylinder
5. Ethanol (Merck<sup>®</sup> KGaA (analyst grade))
6. Copper wire with diameter of 0.50 mm
7. Iron wire with diameter of 0.50 mm
8. Nichrome wire with diameter of 0.50 mm
9. Parafilm
10. 100 % Eucalyptus oil (aromatherapy essential oil)
11. Diesel oil from Central Institute of Forensic Science (CIFS), Thailand



## 3.2 Experimental section

### 3.2.1 Candle casting from paraffin wax

A 1000 g of paraffin wax is heated until it becomes the molten paraffin wax (the melting temperature of paraffin  $\sim 105$  °C). Then, the molten paraffin wax was casted by filling into a stainless steel cylinder of various diameters: 2, 4, 6, and 8 cm. The height of the cylinder was fixed at 10 cm. The candle wick was placed in the middle of the cylinder, and held at room temperature until it was settled into the solid form, the so-called “candle”. These candles were used as CNPs sources.

### 3.2.2 Apparatus setting for CNPs synthesis

A homemade apparatus for flame combustion synthesis of CNPs is shown in Figure 3.1. The candle flame disturbance played a critical role in the CNPs synthesis. In this work, we used grid as the candle flame disturbance which was placed on another o-ring stand above the candle. The cylindrical aluminium plate was held closely to the top side of the grid for collecting the synthesized CNPs.

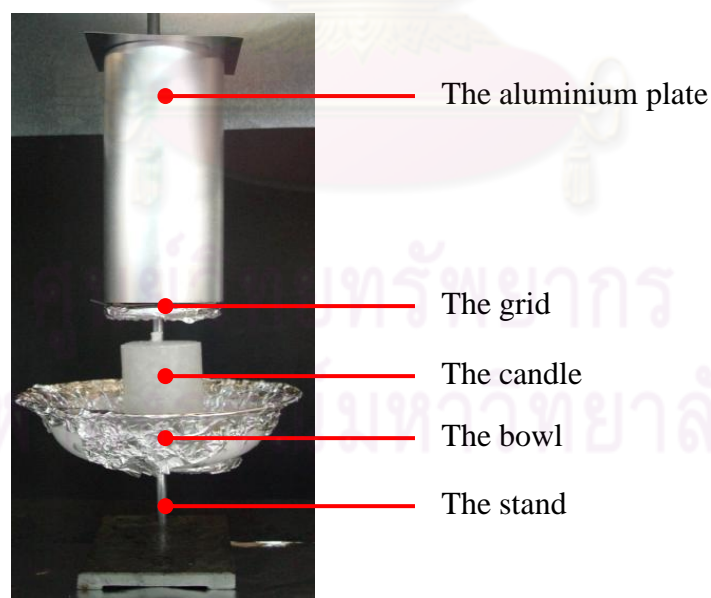


Figure 3.1 The apparatus for CNPs synthesis.

### 3.2.3 Preparation of the grid

The synthesis of CNPs by candle flame combustion technique requires oxygen shortage in order to reach the incomplete combustion condition. The incomplete combustion condition was accomplished by candle flame disturbance. In this work, the grid was used as the flame disturbance. The investigated parameter for finding the optimal condition for CNPs synthesis were grid interval, types of wire, and shape of the grid. The grid interval of 0.1, 0.5, and 1.0 cm were chosen as shown in Figure 3.2. The copper wire, iron wire, and nichrome wire with a diameter of 0.5 mm were used, as shown in Figure 3.3. The suitable wire type was weaved to the various grid shapes i.e. square grid and dome grid (the height of 6.0 cm. and the diameter of 3.0 cm) were shown in Figure 3.4. Each experiment was performed to determine the suitable grid for obtaining the highest yield of carbon nanoparticles.

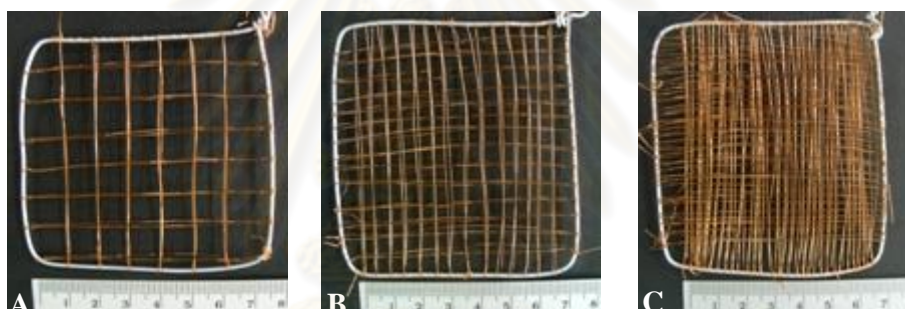


Figure 3.2 The chess square grid with the grid interval of (A) 1.0 cm, (B) 0.5 cm, and (C) 0.1 cm.

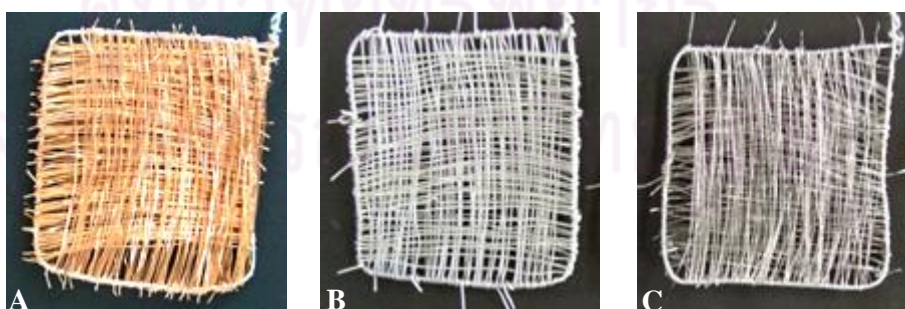


Figure 3.3 The various wire types for grid weaving (A) copper wire, (B) iron wire, and (C) nichrome wire.

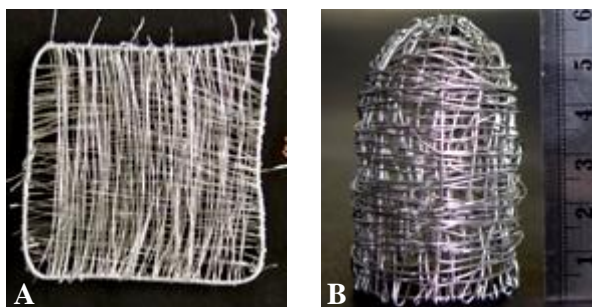


Figure 3.4 The various grid shapes (A) square and (B) dome (the height of 6.0 cm and the diameter of 3.0 cm).

### 3.2.4 The flame disturbance of candle

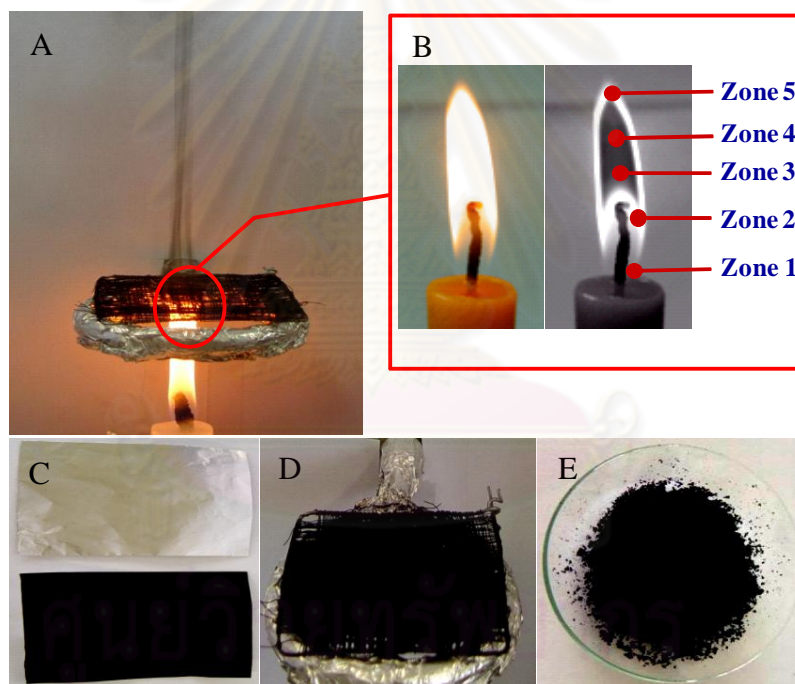


Figure 3.5 The flame combustion of candle wax: (A) the flame disturbance with the grid, (B) the candle flame zone, (C) CNPs on aluminium plate, (D) CNPs on the grid, and (E) CNPs powder.

The candle flame disturbance was performed by inserting grid to the desired flame combustion zone (Figure 3.5A). Generally, the candle flame zone can be classified into five zones (Figure 3.5B), as mentioned in CHAPTER II. In our experiment, the candle flame disturbance was carried out at the regions between zone 2 and 3, zone 3 and 4, and zone 4 and 5. For the regions between zone 1 and 2 were

not yet started the combustion. So, these regions were not used in this experiment. The synthesized CNPs were collected on aluminum plate and on the grid, as shown in Figure 3.5C and 3.5D, respectively. Then, the collected CNPs on aluminum plate and the grid were black powder as shown in Figure 3.5E.

### 3.2.5 The adsorption testing of volatile organic compound by CNPs

#### 3.2.5.1 CNPs pellet casting for adsorption of eucalyptus oil

The synthesized CNPs were black powder, and had light weight. The sample application of the synthesized CNPs was employing them as volatile organic compound adsorber. First of all, they must be casted to pellet in order to be easily utilized for the volatile organic compound adsorbing. For the casting procedure, CNPs powder was first filled into pellet holder and pressed with hydraulic force. After that, CNPs were shaped to pellet (the diameter of 3.0 cm and the thickness of 1 mm). The various conditions were investigated in order to get the optimal pellet as shown in Table 3.1.

Eucalyptus oil was used for testing because it was the common volatile organic compound. The adsorption testing of the volatile organic compound adsorbing was carried out by dropping eucalyptus oil on a filter paper (Whatman<sup>®</sup> Schleicher & Schuell, No.1). Then, it was placed into the same bottle with CNPs pellet. The bottle was sealed by parafilm and stored at room temperature for 24 hours (Figure 3.6). After that, the molecular characteristic of the adsorbed volatile organic compound was investigated with ATR FT-IR microspectroscopy.

Table 3.1 The conditions of CNPs pellet casting for adsorption of eucalyptus oil.

Weight of CNPs powder (g)	Compression (Ton)
0.05	0.5
0.05	1.0
0.05	2.0
0.1	0.5
0.1	1.0
0.1	2.0

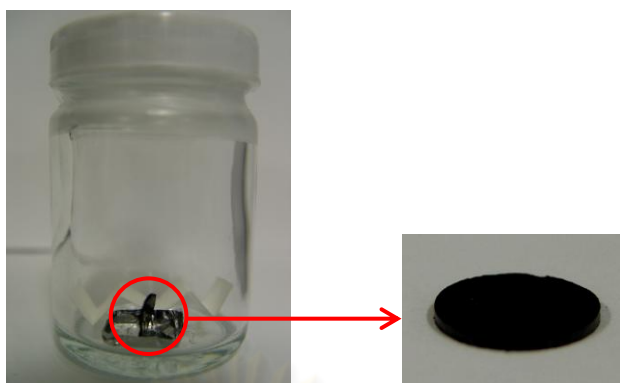


Figure 3.6 CNPs pellet with adsorbed–volatile compound.

### 3.2.5.2 CNPs pellet casting for adsorption of diesel oil

CNPs pellets casted in 3.2.5.1 were easily cracked. Therefore, the binder was added in CNPs pellet casting in order to strengthen it when utilized as volatile organic compound adsorber. The experiment of diesel oil adsorbed by CNPs pellet was done in cooperation with Central Institute of Forensic Science (CIFS), Thailand. The binders for mixing with CNPs powder were Teflon powder and a paper pulp as shown in Tables 3.2 and 3.3, respectively.

Table 3.2 The conditions of CNPs pellet casting with Teflon powder as binder.

Weight of CNPs powder (g)	Weight of Teflon powder (g)	Compression (Ton)
0.01	0.05	1.0
0.01	0.05	1.0
0.01	0.10	1.0
0.01	0.10	1.5
0.05	0.20	2.0
0.05	0.20	2.5
0.10	0.10	3.0
0.10	0.05	1.5



Diesel oil was used for testing because it was the flammable volatile organic compound which used to prove evidence in arson crime. The adsorption testing of the volatile organic compound adsorbing was carried out by dropping diesel oil on the filter paper (Whatman® Schleicher & Schuell, No.1). Then, it was placed in the same bottle with CNPs pellet and sealed rapidly by a bottle cap. It was baked at 95 °C for 24 hours. Then, the pellet was left in vial containing 1 mL of dichloromethane (solvent in the organic compound dissolving on CNPs pellet), and was mixed together by vortex for 1 hour. The molecular characterization of adsorbed volatile organic compound was performed by GC/FID technique.

Table 3.3 The conditions of CNPs pellet casting with paper pulp as binder.

Weight of CNPs powder (g)	Weight of paper pulp (g)	Compression (Ton)
0.10	0.01	1.0
0.10	0.01	1.0
0.10	0.01	1.0
0.10	0.01	1.5
0.05	0.01	2.0
0.05	0.02	1.5
0.05	0.05	1.5
0.05	0.10	1.5

### 3.3 Characterization of CNPs

#### 3.3.1 The molecular information and crystal structure characterization

##### 3.3.1.1 ATR FT-IR microspectroscopy

The synthesized CNPs powder and CNPs pellet for adsorption volatile organic compound were characterized by attenuated total reflection Fourier transform infrared (ATR FT-IR) microspectroscopy. All ATR spectra were collected by a Continuum™ infrared microscope equipped with a mercury-cadmium-tellurium (MCT) detector that attached to the Nicolet 6700 FT-IR Spectrometer. Germanium



(Ge) was used as internal reflection element (IRE). CNPs powder or CNPs pellet was first mounted onto a glass slide and positioned on the microscope stage. For spectral acquisition of samples, the stage of microscope was raised in order to bring sample contact with the tip of Ge  $\mu$ IRE. The ATR spectra of samples were acquired in the reflection mode of infrared microscope. All spectra were measured from 750 to 4000  $\text{cm}^{-1}$  with 64 co-added scans, and the spectral resolution of 4  $\text{cm}^{-1}$ .

### **3.3.1.2 X-ray diffraction (XRD)**

The XRD pattern was used to investigate the crystal structure of synthesized CNPs such as graphite, diamond, and amorphous structure. For sample preparation, CNPs powder were pressed into a sample holder with a smooth plane surface. Then, the prepared samples were put into the sample chamber. XRD analysis used in this work was Rigaku, Dmax 2200/Ultima plus X-ray powder diffraction (XRD) with a monochromator, and Cu  $K_{\alpha}$  radiation (40 kv 30 mA) at angle ( $2\theta$ ) ranging from 10–70 degree. The scan speed was 1 degree/min. The scan step was 0.02 degree. The three slits (scattering, divergent, and receiving slits) were fixed at 0.5 degree, 0.5 degree and 0.15 mm, respectively.

### **3.3.1.3 Raman spectroscopy**

Raman spectroscopic technique was used to investigate the hybridization of the carbon atom of CNPs. Renishaw (invia model) dispersive Raman spectroscope was employed. For sample preparation, CNPs powder were put onto glass slide and placed into the chamber. The sample was bombarded by an Ar ion laser (514 nm). The grating 1,800 L/mm (Vis), exposure times of 25 seconds, and the spectra range of 400-2,500  $\text{cm}^{-1}$  were employed.

#### **3.3.1.4 Gas Chromatography/Flame Ionization Detector (GC/FID)**

The molecular characteristic of the adsorbed volatile organic compound was performed. For sample preparation, CNPs pellet already adsorbed with volatile organic compound was mixed with 1 mL of dichloromethane together by vortex for 1 hour. And then, the filtrated solution was injected in Agilent technologies (6890N Network system) GC/FID. The size of column was 30 m x 320  $\mu\text{m}$  x 0.25  $\mu\text{m}$  (Methyl Siloxan Capillary). The carrier gas was helium. The flow rate of 2 mL/min was used.

### **3.3.2 Morphology analysis/Imaging technique**

#### **3.3.2.1 Scanning electron microscope (SEM)**

Particles size and morphology of CNPs were observed via JSM-6480LV model at 15 kV of accelerating voltage. CNPs samples were prepared by collecting them on aluminium plate by exposing to the soot, which was generated from candle flame disturbance for 2 seconds and 30 seconds and CNPs powder. The CNPs films on aluminium plate and CNPs powder were mounted onto carbon tape on stub. The samples were loaded to sample chamber and then the observation was conducted immediately by image catcher scanner for taking the photograph.

#### **3.3.2.2 Transmission electron microscope (TEM)**

Particles size and morphology of CNPs after ultrasonication were characterized by TEM zero A H-7650 model at 100 kV acceleration voltage. For samples preparation, CNPs were suspended in ethanol by ultrasonication for 15 minutes and another CNPs were suspended in ethanol by ultrasonication for 1 hour. After that, CNPs uniform dispersion was dropped on a Formvar-coated copper grid. The sample was loaded into sample chamber, and then the morphology of samples was analyzed.

### 3.3.2.3 Atomic force microscopy (AFM)

This technique had two samples preparations. The CNPs after sonicating in ethanol for 1 hour were dropped on a cover glass or exposing the coated ethanol with thin film on cover glass directly to the soot which was generated from candle flame disturbance. The dynamic force microscope mode (DFM) was performed on SPI4000/SPA400 (SII NanoTechnology Inc.). Cantilever type was SI-DF20. The scanning area was 0.5  $\mu\text{m}$ –1  $\mu\text{m}$ .

### 3.3.3 Surface area analysis

#### 3.3.3.1 N<sub>2</sub> adsorption/desorption analysis

Surface area of CNPs was determined in term of nitrogen adsorption/desorption isotherm. BET specific surface area of CNPs was evaluated by mean of a BELSORP-II instrument. The CNPs powder weight was 0.009 g and the exact weight pretreatment was weighed at 300 °C for 1 hour before each measurement.

ศูนย์วิทยทรัพยากร  
จุฬาลงกรณ์มหาวิทยาลัย

## CHAPTER IV

### RESULTS AND DISCUSSION



Carbon Nanoparticles (CNPs) in this research were produced by paraffin combustion of candle. Generally, the candle combustion cannot produce CNPs due to the complete combustion changing paraffin to carbon dioxide (CO<sub>2</sub>). However, the disturbance of the combustion pattern has controlled by the amount of the oxygen input supply in the system, CNPs can be generated. The experiment in a stagnant system in order to get the stable flame combustion pattern and generate CNPs was performed. The metal grids were used for the oxygen supply into the flame or reduce the area of the complete combustion of the flame. CNPs were deposited onto an aluminium substrate. Then, CNPs were collected and performed further analysis. The characterizations of CNPs were divided into the molecular information by ATR FT-IR microspectroscopy and Raman spectroscopy. The crystal structure was characterized by X-ray diffraction (XRD). The morphology analysis performed by scanning electron microscopy (SEM), transmission electron microscopy (TEM), atomic force microscopy (AFM). Surface area analysis was investigated by N<sub>2</sub> adsorption/desorption technique. The characterizations of CNPs indicated that the obtained CNPs are nano-size particle with extremely high surface area. The application of these nanoparticles by employing as adsorber for volatile organic compound was explored.

#### 4.1 The diameter of candle wick

The diameter of candle wick affects the transportation of liquid wax to the flame. The candle body with 2.0 cm in diameter with the diameter of candle wick of 0.15 and 0.5 cm are compared. The synthesized CNPs were a fine black powder, and had light weight. The % yields of CNPs were determined as shown in Table 4.1. It was found that the yield of CNPs synthesis with the small and the big candle wick were  $1.05 \pm 0.02\%$  and  $2.05 \pm 0.02\%$ , respectively. From the observation at the steady

state of flame, the small candle wick has the flame size smaller than the big candle wick as shown in Table 4.1. There was no soot or carbon generation. This indicated that the combustion was complete. However, the phenomenon of the big candle wick combustion is more incomplete. Consequently, the amount of carbon particles from a big candle wick is higher. Therefore, the synthesized CNPs from a big candle wick have the yield of CNPs higher than that of the synthesized CNPs from a small wick.

Table 4.1 Comparison of the diameter of candle wick in the synthesis of CNPs.

	Diameter of candle wick (cm)	
	0.15	0.5
The picture of candle wick combustion pattern with difference diameter		
Yield of CNPs (%)	1.05±0.02	2.05±0.02

This synthesis has a low yield of CNPs because CNPs are generated from incomplete combustion. In ambient condition, there is high oxygen content in the air. The combustion of candle is quite complete, so the products are heat, light and mainly carbon dioxide [13]. To promote the incomplete combustion, we had to interfere the system by disturbing the flame. The disturbed flame got a few CNPs quantity comparable to the pyrolysis synthesis which did not consume oxygen in the combustion process. The carbon content of hydrocarbon compound is entirely carbonized [6]. Therefore, pyrolysis synthesis can produce the quantity of CNPs more than the candle flame combustion synthesis.

Figure 4.1A shows the ATR FT-IR spectrum of paraffin wax. It was found that there was only C-H stretching vibration at 2,800-3,000  $\text{cm}^{-1}$  and C-H bending vibration at 1,350-1,480  $\text{cm}^{-1}$  [29] which was the characteristic of wax. It is the original compilation of wax which is a hydrocarbon compound. Paraffin wax was shaped into candle and employed as carbon source in CNPs synthesis. Figures 4.1B and 4.1C show the ATR FT-IR spectra of the synthesized CNPs from candle wick with diameters of 0.15 cm and 0.5 cm, respectively. It was found that the synthesized CNPs did not reveal any peak which associated to wax spectrum—any carbonyl (C=O), hydroxyl (O-H) and the other carbon species that are formed with oxygen or hydrogen. There is C=C stretching vibration at 1,580  $\text{cm}^{-1}$  which corresponds to the literature report of C=C stretching vibration of the general carbon material at 1,570-1610  $\text{cm}^{-1}$  [30]. The synthesized CNPs from various diameters of candle wick are possibly pure CNPs.

This spectrum also shows the differential type peak shape at 1580  $\text{cm}^{-1}$  which suggests wavenumber from the inflection point of the differential type peak shape. It can be explained by extraordinary high refractive index of CNPs. Due to the attenuated total reflection (ATR) phenomenon, the evanescent wave (the part of the light passes the crystal interface and interacts with a sample placed in a close contact with the Ge  $\mu$ IRE.) travelling in an optically dense medium strikes the boundary of a second medium with a relatively lower refractive index at a certain angle greater than the critical angle. In this case, Ge  $\mu$ IRE and CNPs have refractive index ( $n$ ) of 4.0 and 2.4, respectively [31]. It was found that the critical angle calculated by Snell's law is 37°. It is greater than the angles of incidence ranging from 15° to 35° [32] of the focused radiation rays in microscope. Therefore, ATR does not contribute to all spectrum and there is differential type peak shape.

The next experiment is carried out by varying the ratio of diameter of the candle wick and candle body in order to find the optimal condition of the synthesis for the highest quantity of production and the highest purity of CNPs.



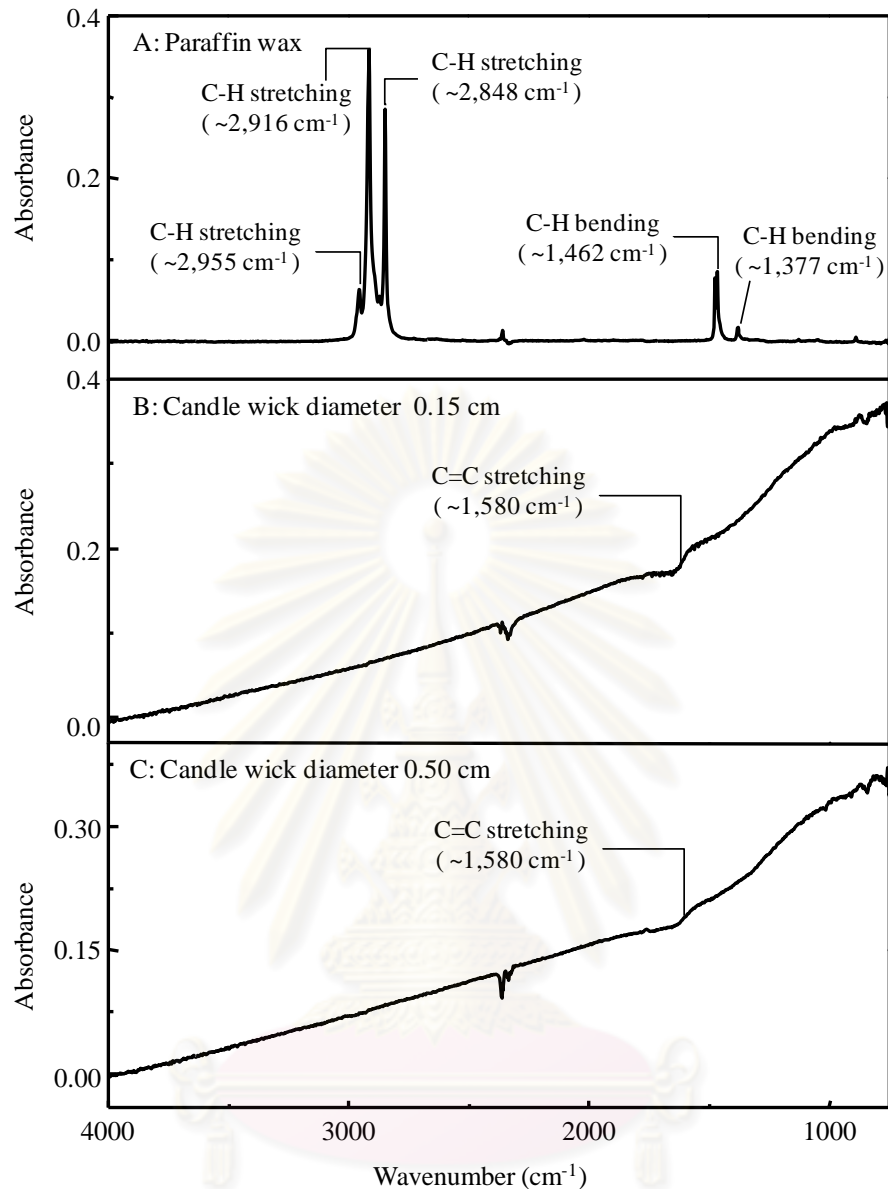


Figure 4.1 ATR spectra of paraffin wax and CNPs from the synthesis with candle wick of each diameters: (A) paraffin wax, (B) the diameter of 0.15 cm, and (C) the diameter of 0.5 cm.





#### 4.2 The ratio of diameter of candle wick and candle body

In this part, the effect of the ratio of diameter of candle wick and candle body on CNPs synthesis are concerned. The diameter of the candle wick is 0.5 cm while the diameters of candle body are 2, 4, 6, and 8 cm. The flame sizes of each candle are not different since the size of flame depends only on the diameter of candle wick. The

synthesized CNPs of each diameter ratio are analyzed by ATR FT-IR microspectroscopy.

ATR FT-IR spectra of the synthesized CNPs from the diameter ratio of candle of 0.5:4, 0.5:6, and 0.5:8 has a characteristic of wax in their spectra. There are C-H stretching vibration at  $2,800\text{--}3,000\text{ cm}^{-1}$  (Figure 4.2B, 4.2C, and 4.2D). The characteristic of wax in the observed spectra is the consequence of non-combusted volatile wax during the combustion process. As the wax is being melted by the candle flame, the melted wax is adsorbed and drawn up to the flame through the wick by capillary force. If the supply rate of wax through the wick is more than the rate of combustion, some of the wax will not be combusted by the candle flame, and the synthesized CNPs will be contaminated by the residual of non-combusted volatile wax. On the other hand, when the diameter ratio of 0.5:2 is employed, there is no C-H stretching vibration, which is the characteristic of wax, in the spectrum. This is because the melted wax can be completely combusted. The synthesized CNPs from diameter ratio of candle of 0.5:2 are, then, pure CNPs.

Table 4.2 The candle flames of each diameter ratio of candle wick and candle body in CNPs synthesis.

The diameter ratio of candle wick and candle body (cm:cm)			
0.5:2	0.5:4	0.5:6	0.5:8
			

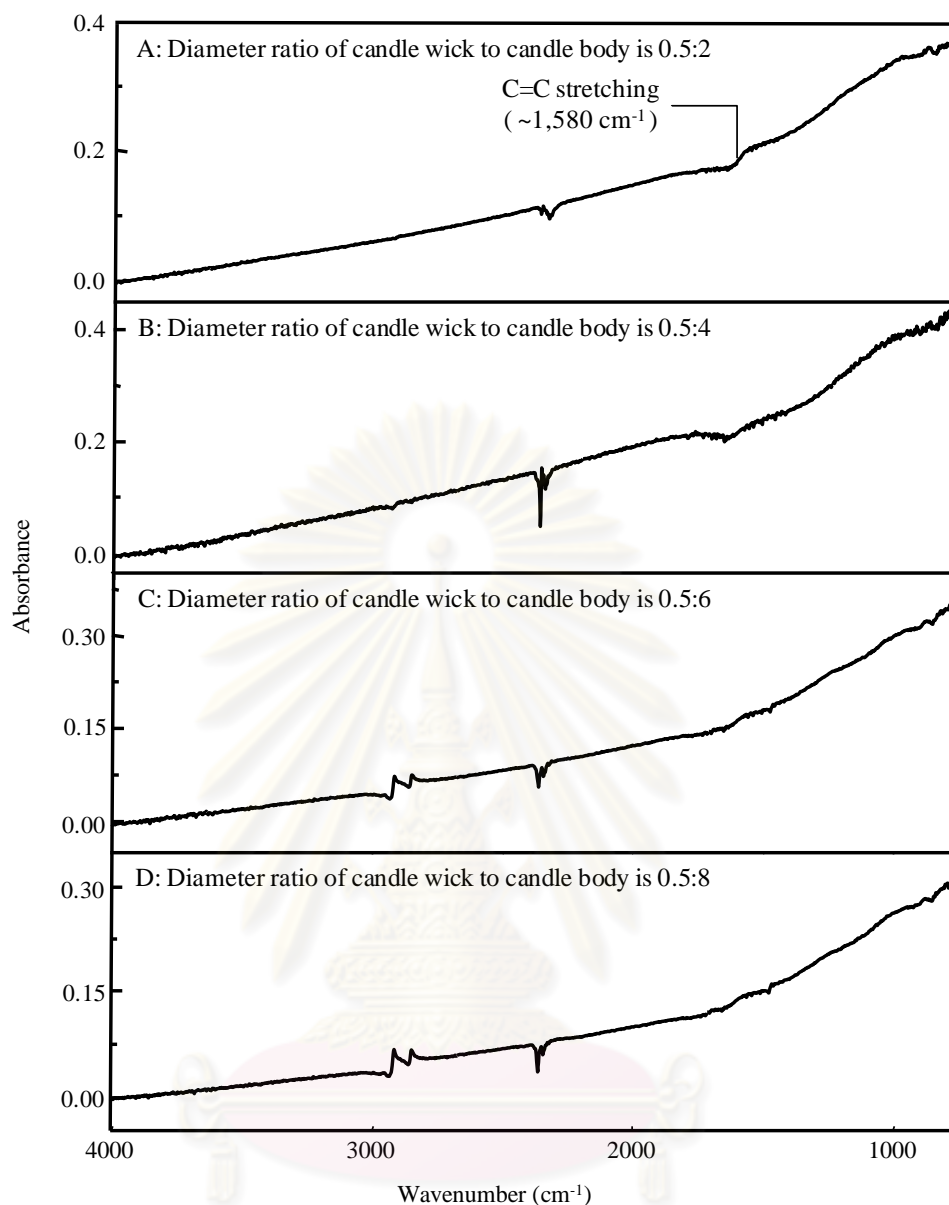


Figure 4.2 ATR spectra of CNPs from the synthesis with diameter ratio of candle wick to candle body (cm:cm) (A) 0.5:2, (B) 0.5:4, (C) 0.5:6, and (D) 0.5:8.

From this experiment, it suggested that the optimal diameter ratio of candle wick to candle body should be 0.5:2. The candle flame from this candle is stable, and the rate of combustion and adsorption of melted wax are in equilibrium. The next experiment will focus on the effect of the length of candle wick above the top surface of the candle body on CNPs production.

### 4.3 The length of candle wick above the top surface of candle body

In this experiment, the optimal diameter ratio of candle (0.5:2) was used for investigating the stability of candle flame with the various length of candle wick. The candle wick length of 0.5, 1.0, 1.5, 2.0, 2.5 and 3.0 cm were chosen. It was found that the candle wick lengths of 1.5, 2.0, 2.5, and 3.0 cm (Figure 4.3C-4.3F) required the longer period of time before obtaining the stable flame than the candle wick lengths of 0.5 and 1.0 cm (Figure 4.3A and 4.3B). From the figures can see that the length of candle wick of 1.5–3.0 cm required some short period of time for the combustion of candle wick before reaching the top surface of the candle, while that of 0.5 and 1.0 cm did not. When the lengths of candle wick were 0.5 and 1.0 cm, the ignited candle flame immediately reaching the top of the candle surface. The combustion process was begun instantly. The molten wax was continuously consumed and combusted until the supply rate of wax through the wick and the rate of combustion were equal. The stable flame was obtained. However, when the length of candle wick was in the range of 1.5–3.0 cm, there was some temperature reduction after the ignited candle flame reached the top of the candle surface (see Figure 4.3C-4.3F at the time around 200 seconds). This was because some of the thermal energy was required for melting the candle wax before the usual combustion process began. Ultimately, all of the candle wick lengths yielded the stable flame (the height of 13 cm). However, the candle wick length of 1.0 cm in CNPs synthesis was chosen, since the time required for obtaining the stable flame is short, and this candle wick length was easier to ignite than that of 0.5 cm. Therefore, the most suitable candle wick length in CNPs synthesis was 1.0 cm.

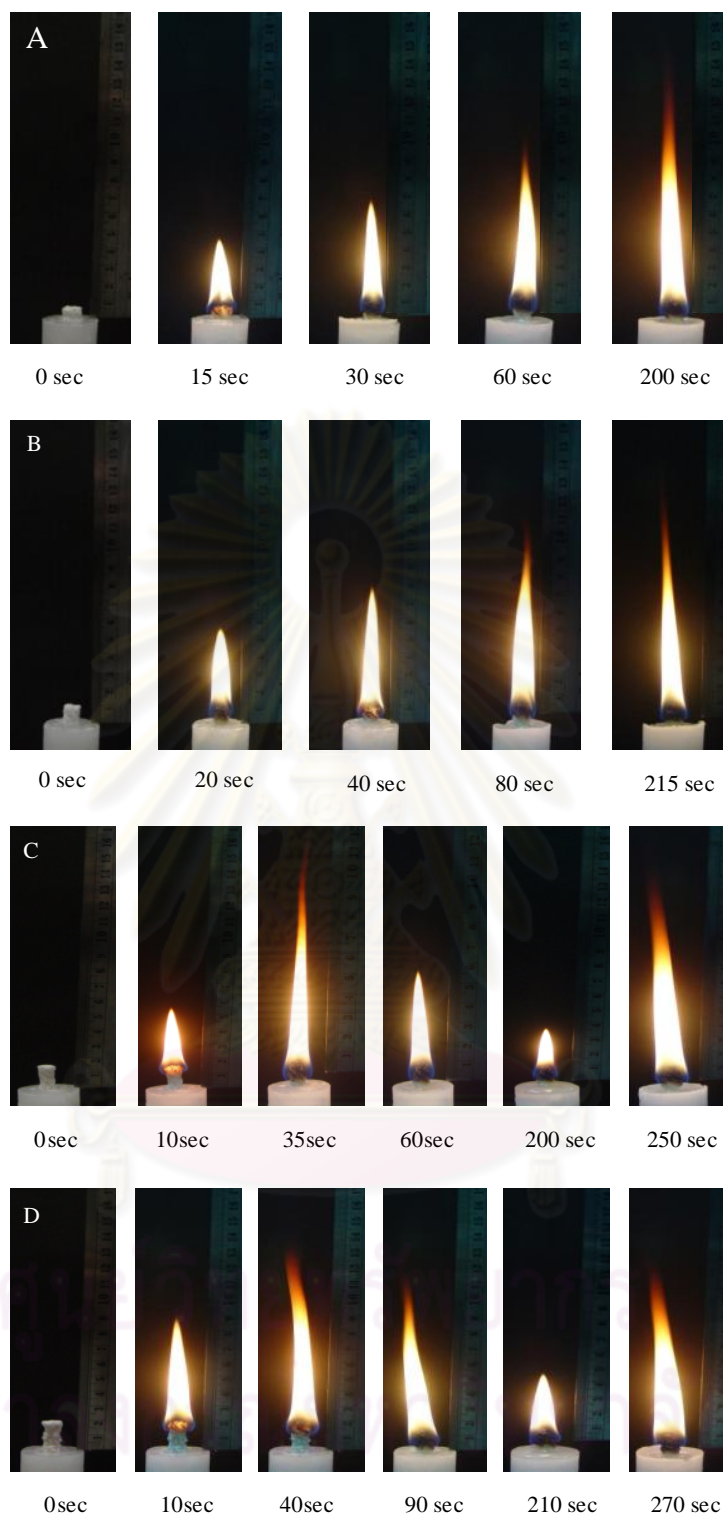


Figure 4.3 The combustion of various lengths of candle wick: (A) 0.5 cm, (B) 1.0 cm, (C) 1.5 cm, (D) 2.0 cm, (E) 2.5 cm, and (F) 3.0 cm.

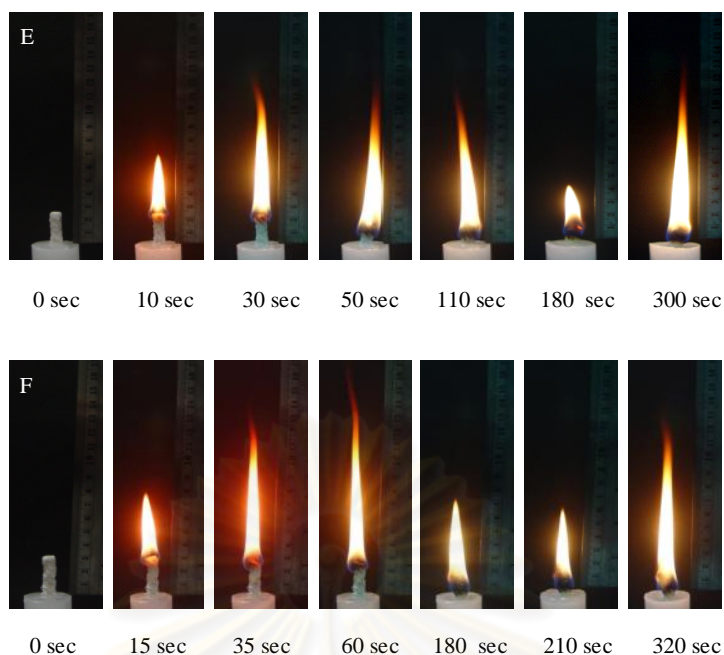


Figure 4.3 (continued) The combustion of various lengths of candle wick: (A) 0.5 cm, (B) 1.0 cm, (C) 1.5 cm, (D) 2.0 cm, (E) 2.5 cm, and (F) 3.0 cm.

#### 4.4 The candle flame disturbance of each flame zone

Naturally, if candle flame disturbance is not applied, carbon particles in flame will react directly with oxygen and form carbon dioxide. Consequently, CNPs are not generated. The candle flame disturbance is essential for synthesizing CNPs because it will reduce the area of reaction between carbon particles and oxygen. The candle flame can be classified into 5 zones which each zone has different combustion process as mentioned in CHAPTER II. The flame disturbance zone is the limiting factor whether pure or impure CNPs will be produced. Here, glass slide is used as flame disturber. Soot or CNPs have been deposited on glass slide after they are generated. The candle flame disturbance between the second and the third zone, the third and the fourth zone, and the fourth and the fifth zone are compared.



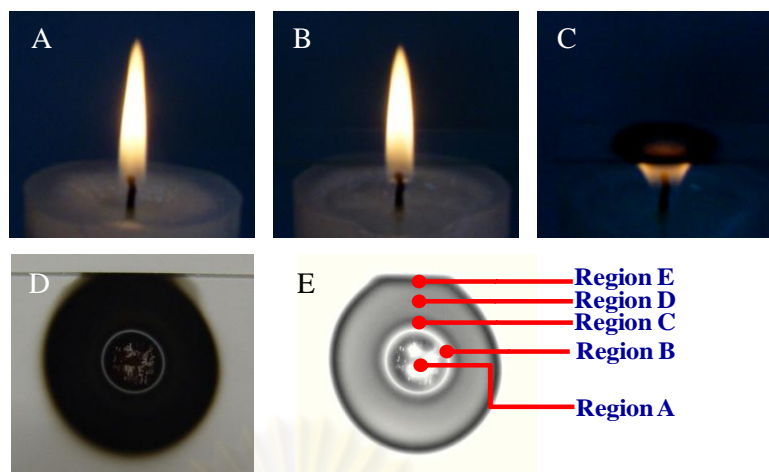


Figure 4.4 The disturbed candle flame between the second and the third zone (A) The candle flame which is not disturbed, (B) The inserted glass slide at the position of the candle flame disturbance, (C) The candle flame disturbance between the second and the third zone by glass slide, (D) CNPs film on glass slide after the candle flame disturbance, and (E) The processed image of CNPs film.

The candle flame disturbance between the second and the third zone is shown in Figure 4.4A-4.4C. The thin CNPs film deposited on glass slide has various regions as shown in Figure 4.4D. The image of CNPs film does not reveal any distinct regions. Therefore, the image of CNPs film is processed in Adobe Photoshop program in order to see the apparent difference of various regions of CNPs film as shown in 4.4E. It is found that CNPs film can be classified into five regions labeled as A, B, C, D, and E. The characteristic of each region of CNPs film are characterized by ATR FT-IR microspectroscopy.

ATR FT-IR spectra suggested that CNPs film in the same region have similar spectra. The spectra of the identical regions are collectively shown as a single spectrum. In region A to region D, ATR spectra show characteristic of wax at 2,800–3,000  $\text{cm}^{-1}$  from C-H stretching vibration. This indicates that there are non-combusted volatile waxes in these regions, which correspond to the flame zone in the combustion flame processes in the first to the fourth zone as mentioned in CHAPTER II. In region A reveals the first flame zone, regions B reveals the second flame zone, region C reveals the third flame zone, and region D reveals the fourth flame zone. In the case of

the fourth flame zone, it shows characteristic of wax because the evaporated wax from the third flame zone is mixed together with CNPs film in this flame zone. Another character in the spectra was glass slide character. It is Si-O-Si stretching at 1,010-1,090  $\text{cm}^{-1}$  [29] as shown in Figure 4.5. The glass slide character appears because the evanescent wave passes the Germanium (Ge)  $\mu\text{IRE}$  and penetrates through CNPs film. This indicates that CNPs film is thin, since the thickness of the film is less than the penetration depth of the evanescent wave (A typical IRE has a sampling depth on the order of 0.5 to 3.5  $\mu\text{m}$ , so the analyzed sample should be thinner than those) [32]. However, the spectrum of region E does not show glass slide character because CNPs film in this region are thicker than these in the other regions, and thicker than the sampling depth of the ATR technique. In addition, complete combustion of wax occurs in the fifth zone. The wax character is not observed in spectrum. There is only carbon character. It is C=C stretching vibration at 1,580  $\text{cm}^{-1}$  which corresponds to the literature report in section 4.1 as shown in Figure 4.5. In summary, the candle flame zone between the second and the third zone are the starting zone of wax combustion. The burning of wax are incomplete. It still remains wax character in this zone. Therefore, the synthesized CNPs from the candle flame disturbance between the second and the third zone are not pure CNPs.

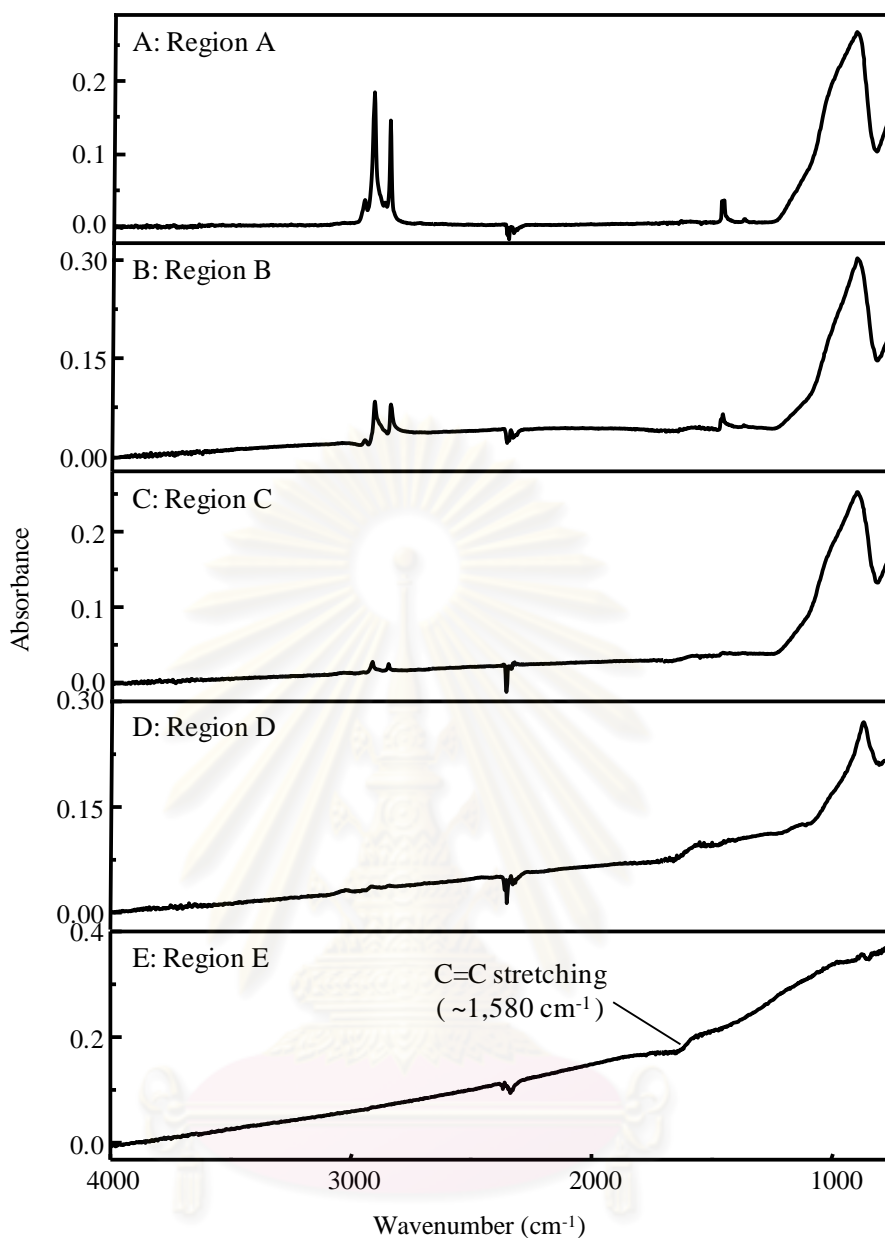


Figure 4.5 ATR spectra of various regions of CNPs film on glass slide by the candle flame disturbance between the second and the third zone.

Figure 4.6 shows the candle flame disturbance between the third and the fourth zone which have flame disturbance process as same as the candle flame disturbance between the second and the third zone. CNPs film from the candle flame disturbance classified into four regions labeled A, B, C, and D. The characteristic of each region of CNPs film were characterized by ATR FT-IR microspectroscopy.

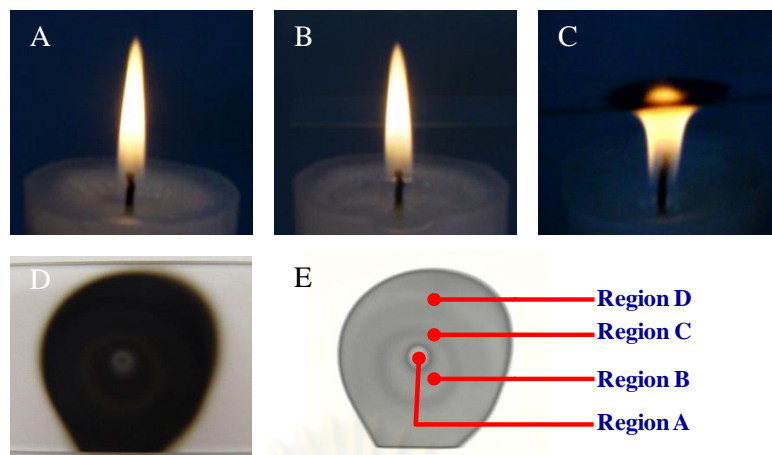


Figure 4.6 The disturbed candle flame between the third and the fourth zone (A) The candle flame which is not disturbed, (B) The inserted glass slide at the position of the candle flame disturbance, (C) The candle flame disturbance between the third and the fourth zone by glass slide, (D) CNPs film on glass slide after the candle flame disturbance, and (E) The processed image of CNPs film.

CNPs film from this flame zone disturbance corresponds to CNPs film of the candle flame disturbance between the second and the third zone but there is the difference number of region which has four regions. Additionally, ATR FT-IR spectra of regions A to D give a similar spectra with regions B to E of the candle flame disturbance between the second and the third zone. In regions A to C reveals the second to the fourth flame zone and region D reveals the fifth flame zone. Therefore, the synthesized CNPs from the candle flame disturbance between the third and the fourth zone are not yet pure CNPs.

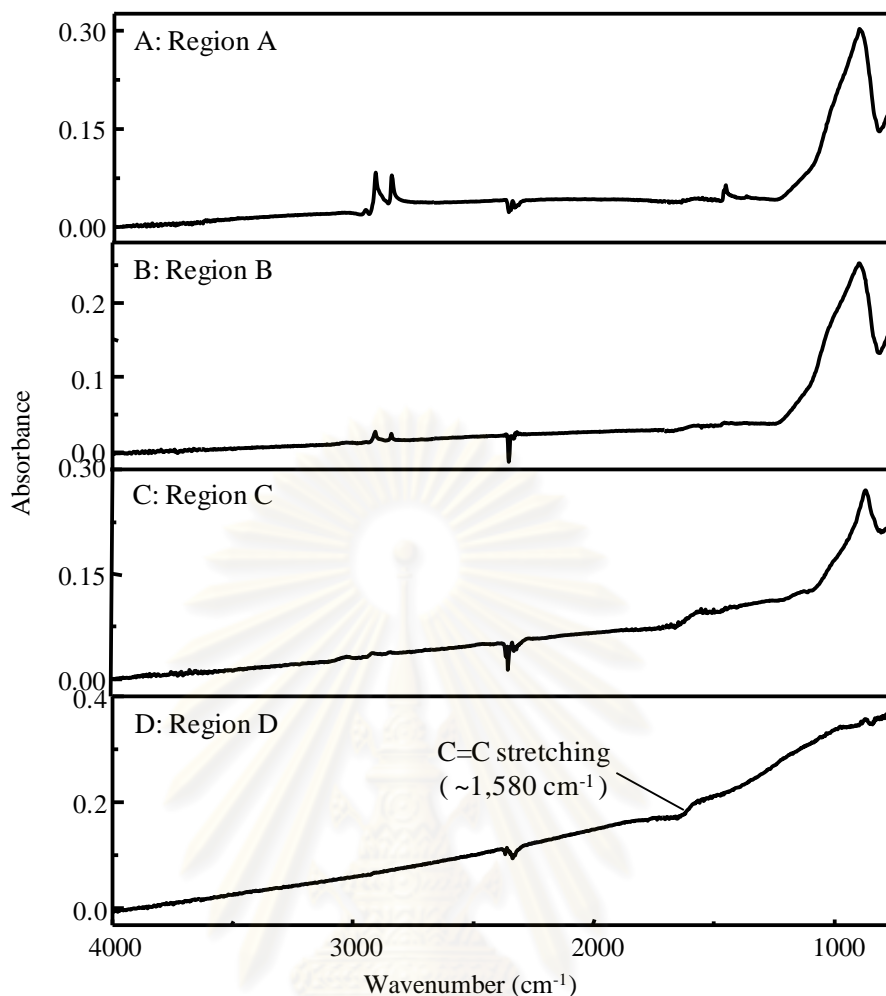


Figure 4.7 ATR spectra of various regions of CNPs film on glass slide by the candle flame disturbance between the third and the fourth zone.

The candle flame disturbing between the fourth and the fifth zone is shown in Figure 4.8A-4.8C. The thin CNPs film deposited on glass slide had various regions as shown in Figure 4.8D. The image of CNPs film was processed in Adobe Photoshop program as shown in 4.6E. It was found that CNPs film can be classified into four regions labeled A, B, C, and D. The characteristic of each region of CNPs film were characterized by ATR FT-IR microspectroscopy.

Figure 4.8 shows the candle flame disturbance between the fourth and the fifth zone which have flame disturbance process as same as the previous candle flame disturbance. But the image of CNPs film did not reveal any distinct regions. Therefore, the image of CNPs film was processed in Adobe Photoshop program in

order to see the apparent difference of various regions of CNPs film as shown in 4.8E. It was found that the processed image of CNPs film did not show any distinct region comparable to CNPs film of the candle flame disturbance between the second and the third zone and the third and the fourth zone. CNPs film was characterized by ATR FT-IR microspectroscopy by linear mapping with  $\mu$ IRE along its diameter.

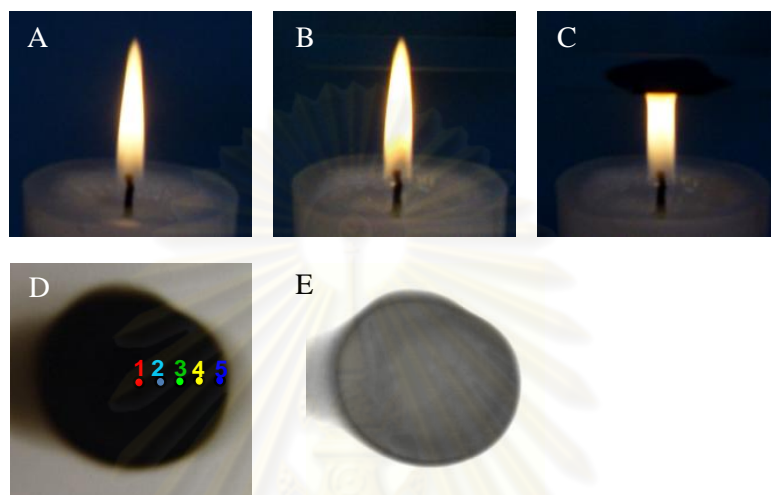


Figure 4.8 The disturbed candle flame between the fourth and the fifth zone (A) The candle flame which is not disturbed, (B) The inserted glass slide at the position of the candle flame disturbance, (C) The candle flame disturbance between the fourth and the fifth zone by glass slide, (D) CNPs film on glass slide after the candle flame disturbance, and (E) The processed image of CNPs film.

ศูนย์วิทยทรัพยากร  
จุฬาลงกรณ์มหาวิทยาลัย



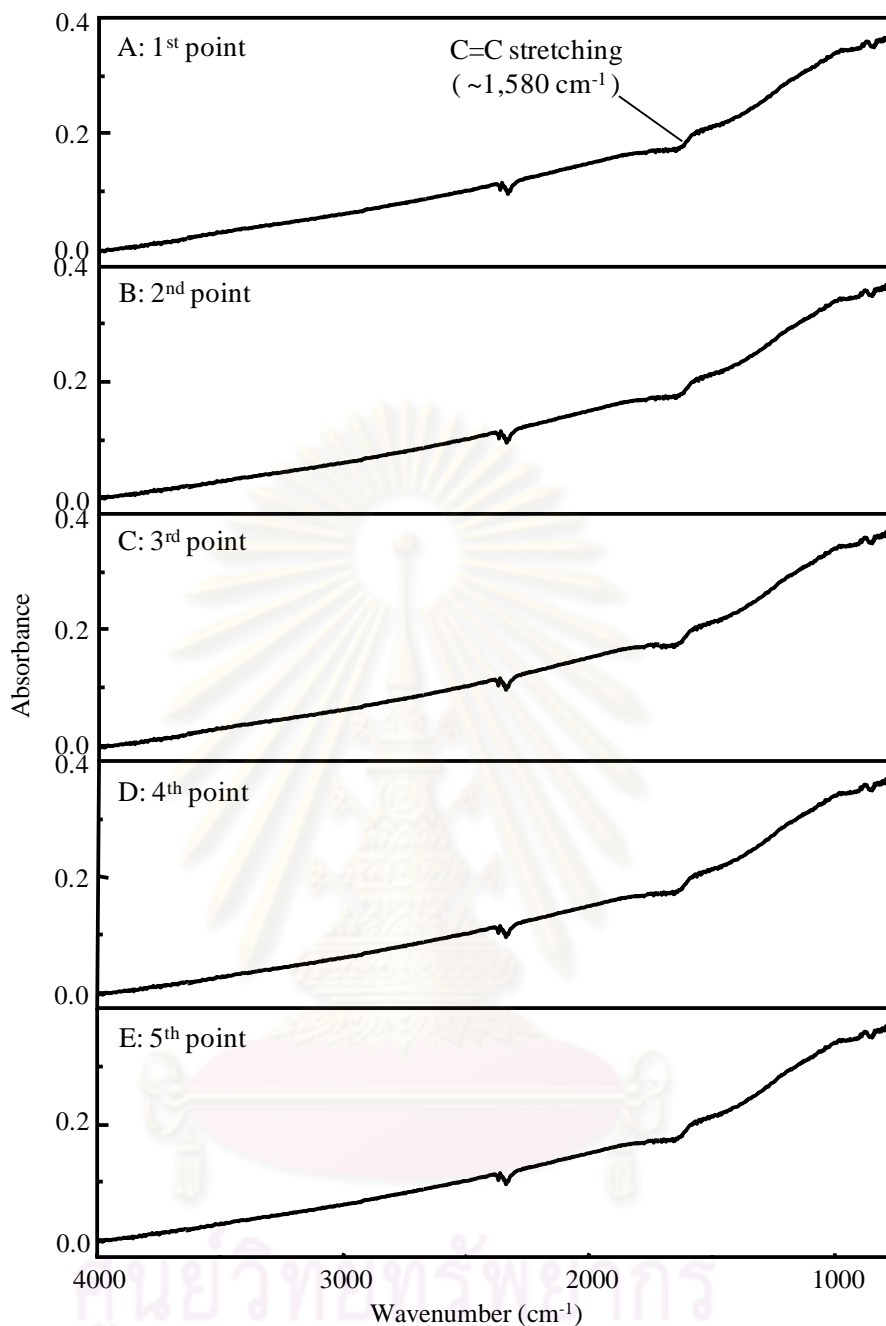


Figure 4.9 ATR spectra of CNPs films along its diameter on glass slide by the candle flame disturbance between the fourth and the fifth zone.

ATR spectra as shown in Figure 4.9 suggest that CNPs film from along its diameter have similar spectra for each sampling position. There is no glass slide character in the spectrum. CNPs film is thicker than the sampling depth of the ATR technique [32]. The disturbed candle flame between the fourth and the fifth zone yields the uniform CNPs film. There is the similarity in molecular structures of carbon

character. It is C=C stretching vibration at  $1,580\text{ cm}^{-1}$ . There is no characteristic of wax remaining comparable to the candle flame disturbance between the second and the third zone and the third and the fourth zone. This indicates that there is no non-combusted volatile wax in these regions. Therefore, the synthesized CNPs by the candle flame disturbance between the fourth and the fifth zone are pure CNPs.





From this experiment, it suggests that the position of the candle flame disturbance is very important for the synthesis of CNPs because it can produce the pure CNPs and increase the amount of CNPs. In the next experiment, grid weaving, or candle flame disturber pattern will be investigated.

#### **4.5 The grid interval of candle flame disturbance**

From the candle flame disturbance experiment by glass slide, the disturbance between the fourth and the fifth zone produces pure CNPs. The flame disturber is very important in CNPs synthesis. The candle flame disturbance temperature between the fourth and the fifth zone is  $1,200\text{-}1,400\text{ }^{\circ}\text{C}$ . If aluminium plate is used as the flame disturber. The synthesized CNPs will form on the aluminium plate and be destroyed or melted. It leads to lose the synthesized CNPs. In this experiment, the copper wires were weaved to be chess square having grid intervals of 0.1, 0.5, and 1.0 cm in order to have the least effect with the synthesized CNPs losing.

Laser light is used to observe the light scattering of CNPs synthesized from the candle flame disturbance by various grid intervals. If there is no laser light scattering, it indicates that there is no CNPs formation as shown in Table 4.3. The grid with interval of 0.1 cm can produce soot or CNPs more than that of 0.5 and 1.0 cm as observed via laser intensity. Moreover, % yield of carbon synthesized by the grid with interval 0.1 cm is  $2.10 \pm 0.03$ , but in the case of the grid interval 0.5 and 1.0 cm, % yield is just  $1.02 \pm 0.01$  and  $0.70 \pm 0.03$ , respectively. This is because the grid with interval of 0.1 cm has high surface area in touching with grid of candle flame. It can reduce the area of reaction between carbon particles and oxygen to form carbon dioxide more than the grid interval of 0.5 and 1.0 cm. Therefore, the optimal grid interval is 0.1 cm.

Table 4.3 The candle flame disturbance by various grid intervals and yield of CNPs (%).

Grid interval (cm)	Image of candle flame	Yield of CNPs (%)
No grid		-
1.0		$0.70 \pm 0.03$
0.5		$1.02 \pm 0.01$
0.1		$2.10 \pm 0.03$

From this experiment, it suggests that the grid interval of 0.1 cm can produce a lot of CNPs. The materials used to be a wire may also affect CNPs production. Therefore, the various materials i.e., copper, iron, and nichrome will be weaved as a grid with interval 0.1 cm and CNPs productions will be compared.

#### **4.6 The effect of material of grid on candle flame disturbance**

The candle flame disturbance can produce CNPs by reducing the area of combustion of carbon particles and oxygen between the fourth and the fifth zones. This is because the synthesized CNPs were also collected on grid. So, the material of grid wire is essential to protect the synthesized CNPs losing which occurred from the heat within wire of the candle flame disturbance. Since, the candle flame disturbance temperature between the fourth and the fifth zone is 1,200-1,400 °C, it can destroy or melt the synthesized CNPs and leads to the loss of synthesized CNPs. The optimal mesh grid interval of 0.1 cm is used and copper, iron, and nichrome wire are observed. The %yield of carbon from nichrome wire is  $3.66 \pm 0.03$  more than that of copper and iron wire ( $2.07 \pm 0.03$  and  $2.06 \pm 0.02$ , respectively as shown in Table 4.4). The nichrome wire has thermal conductivity of  $12 \text{ Wm}^{-1}\text{K}^{-1}$  [33] which is less than that of thermal conductivity of copper and iron wires as shown in Table 4.4. It indicates that the nichrome wire has lower ability to flow the heat in wire than copper and iron wire due to the thermal equilibrium reaching of nichrome wire is slow. When the nichrome wire grid was used in synthesis, a lot of CNPs could be produced. Therefore, the optimal wire in grid weaving is nichrome wire.

The various grids weaving shape may also affect CNPs production. In the next experiment, grid weaving shapes of square and dome shapes by nichrome wire weaving will be investigated.

Table 4.4 Thermal conductivity ( $\text{Wm}^{-1}\text{K}^{-1}$ ) and yield of CNPs (%) of the various wire types of the grid weaving in candle flame disturbance.

Wire type	Thermal conductivity ( $\text{Wm}^{-1}\text{K}^{-1}$ ) [33]	Yield of CNPs (%)
Copper wire	401	$2.07 \pm 0.03$
Iron wire	80.2	$2.06 \pm 0.02$
Nichrome wire	12	$3.66 \pm 0.03$



#### 4.7 The grid shape in the candle flame disturbance

The various grid shapes may affect the area of reaction between carbon particles and oxygen. % Yield of CNPs from square grid is  $3.66 \pm 0.03$ , which is greater than that of the dome grid which is  $2.63 \pm 0.02$  as shown in Table 4.5. This is because the square grid shape has wide surface area of grid for expanding the candle flame which can be collected CNPs on grid more than that of narrow surface area of grid. CNPs formation is more favorable than the dome grid shape. In addition, this can also be observed from laser intensity image which the square grid shape had laser intensity more than the dome grid shape when was used to synthesize CNPs as shown in Table 4.5.

By optimizing all factors which have the effects on the synthesis of CNPs by mean of flame combustion technique, the optimal factors are summarized as follows:

- The ratio between diameter size of candle wick and candle wax body is 0.5:2.
- The length of candle wick above the surface of the candle body is 1.0 cm.
- The candle flame disturbance is carried out with grid between the fourth and the fifth zone.
- The grid interval is of 0.1 cm.
- The material of grid wire is nichrome wire.
- The grid shape is square shape.

Table 4.5 Yield of CNPs (%) on disturbance grid.

The grid shape	Image of burning flame	Yield of CNPs (%)
Square		$3.66 \pm 0.03$
Dome		$2.63 \pm 0.02$

## 4.8 The characterizations of CNPs

### 4.8.1 The molecular information and crystal structure characterization

#### 4.8.1.1 ATR FT-IR microspectroscopy

Functional groups of incomplete combustion of reactant for CNPs synthesis from candle are monitored by ATR FT-IR microspectroscopy. ATR spectrum of carbon reveals the differential type peak shape as shown in Figure 4.10 which is explained in section 4.1. It reveals carbon character. It is C=C stretching vibration at  $1580\text{ cm}^{-1}$ . No C-H stretching vibration at  $2,800\text{--}3,000\text{ cm}^{-1}$  and C-H bending vibration at  $1,350\text{--}1,480\text{ cm}^{-1}$ —which is the wax character are observed or there is no non-combusted volatile wax contaminating in the synthesized CNPs. This indicated that there was complete burning of wax as a result there was no wax residue in system. Since the synthesis of CNPs by flame combustion technique is used the



optimal factors in synthesis as shown in section 4.1-4.7. Therefore, the synthesized CNPs are highly pure carbon.

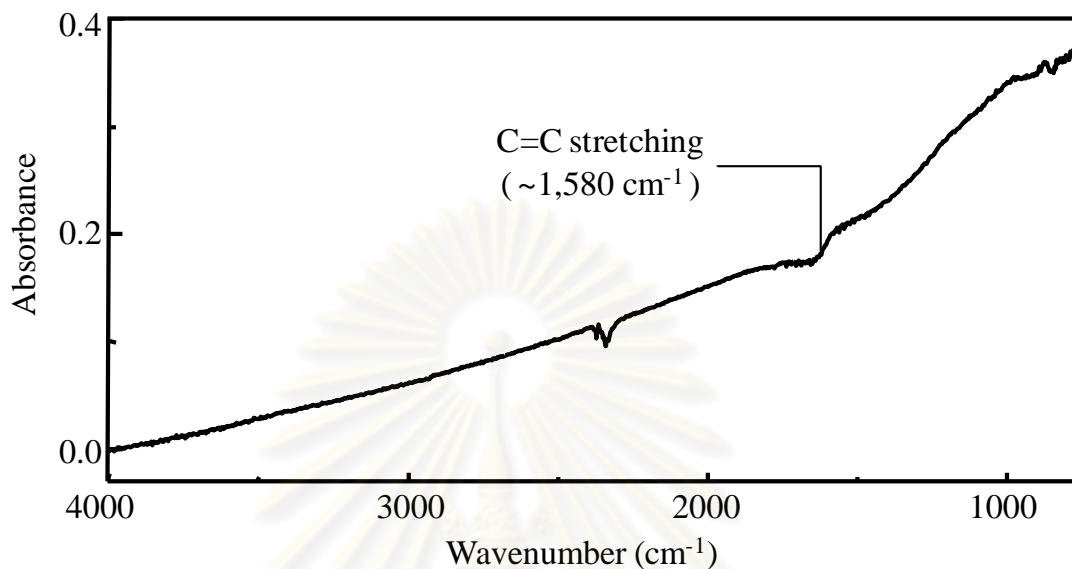


Figure 4.10 ATR spectrum of the synthesized CNPs.

#### 4.8.1.2 X-ray diffraction (XRD)

XRD is a powerful technique for observing the graphitic crystallite of carbon. The XRD pattern of the synthesized CNPs has the [002] and [100] diffraction peak as shown in Figure 4.11A. The broad [002] reflection at  $24.5^\circ$  indicates small domains of coherent and parallel stacking of the graphene sheets. The broad [100] reflections at  $43^\circ$  indicate the presence of honeycomb structure formed by  $sp^2$  hybridized carbon [34]. These two broad peaks are assigned to typical graphitic [002] and [100] diffraction peaks in correspondence with diffraction peaks of disorder carbon structure of a previous work as shown in Figure 4.11B [35]. Therefore, the synthesized CNPs have disorder graphite structure (the stacking of the graphene sheets has random orientation). This structure appears because the mechanism of soot or CNPs formation getting started from small graphite-like sheets stacking together to form particles which cannot form to the perfect graphite structure of carbon. Therefore, Raman technique was used to analyze the other structure of the synthesized CNPs in next characterization.

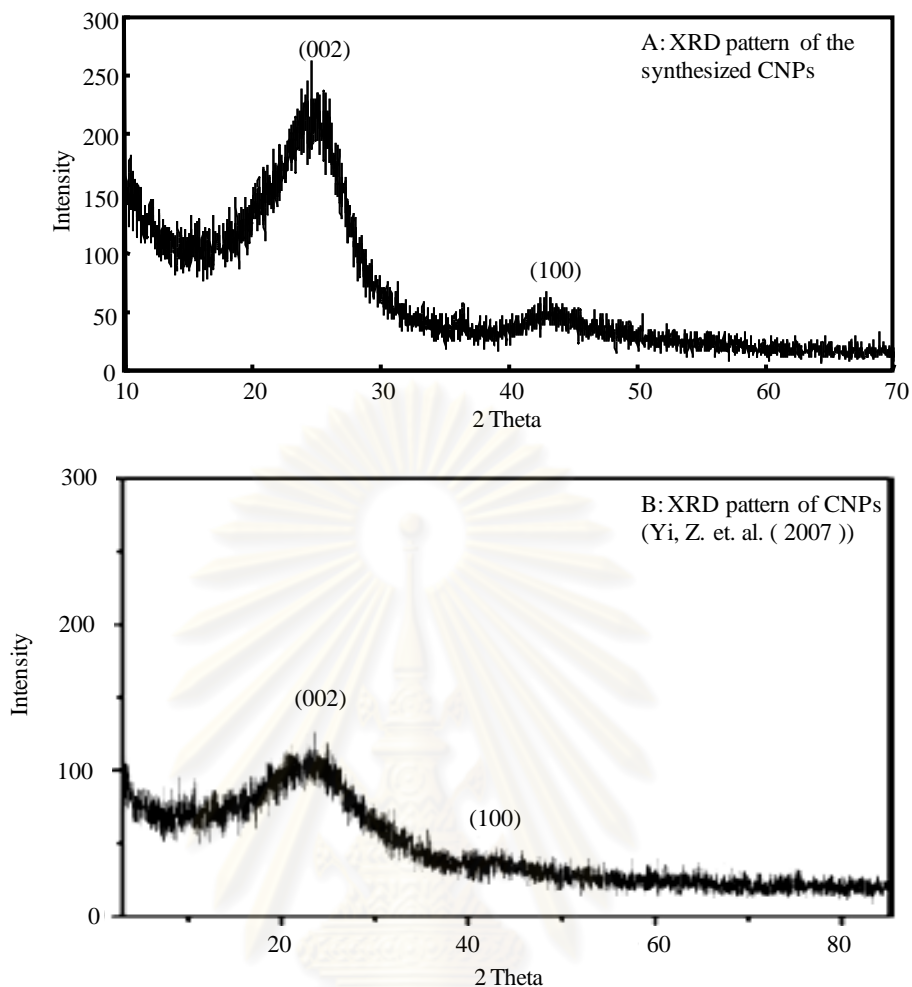


Figure 4.11 XRD pattern of CNPs with (A) the synthesized CNPs and (B) CNPs (Yi, Z. et. al. ( 2007 )).

#### 4.8.1.3 Raman spectroscopy

Raman spectroscopy is one of the most powerful techniques for characterizing carbon materials. In the case of the Raman spectrum for CNPs, two peaks can be found in the wavenumber between  $1,200$  and  $1,800\text{ cm}^{-1}$ . One peak is  $1,500$ - $1,600\text{ cm}^{-1}$  (Graphite band, G band) arises from an in-plane oscillation of carbon atoms in the  $sp^2$  graphene sheet [31]. Another peak is  $1,300$ - $1,400\text{ cm}^{-1}$  (Disordered band, D band) reflecting the degree of defects or dangling bonds contained in the  $sp^2$  arrangement of graphene sheet [31]. The Raman spectra of the synthesized CNPs demonstrate two peaks at  $1,355$  and  $1,597\text{ cm}^{-1}$  (Figure 4.12A). The peak at  $1597\text{ cm}^{-1}$  referred to the G band which indicated graphite structure.

When disorder is introduced into the graphite structure, the broad peak is found at  $1,355\text{ cm}^{-1}$  (D band). In order to achieve the accuracy in the determination of spectroscopic parameters, a curve fitting was used for each spectrum and fitted with Gaussian and Lorentzian functions as shown in Figure 4.12B. It was found that there was a broad peak at  $1,548\text{ cm}^{-1}$ . The result of this fitting is in agreement with the result of a previous work which shows a broad peak around  $1,500\text{-}1,550\text{ cm}^{-1}$  [36]. This broad feature was assigned to amorphous phase. Therefore, Raman spectra of the synthesized CNPs revealed graphite, disorder of graphite and an amorphous structure which occur from the mechanism of CNPs formation [15]. The result of Raman technique agrees with the result of XRD technique which indicates disorder of graphite structure of the synthesized CNPs.

The percentage of each structure is calculated from peak area of the fitted curve. It is found that the synthesized CNPs are the mixture of disorder graphite, graphite, and an amorphous structure. There was 71.03%, 21.44%, and 7.53% of disorder graphite, graphite, and an amorphous structure in the synthesized CNPs, respectively. The major structure is the disorder graphite because the temperature in the CNPs synthesis was lower than the temperature of the highly oriented graphite (perfect graphite) formation ( $2,000\text{-}3,000\text{ }^{\circ}\text{C}$ ) [37]. The synthesized CNPs can be produced from the candle flame disturbance between the fourth and the fifth zone which have the flame temperature  $1,200\text{-}1,400\text{ }^{\circ}\text{C}$ . Therefore, the percentage of disorder graphite structure is greater than that of the percentage of graphite and amorphous structure.

ศูนย์วิทยทรัพยากร  
จุฬาลงกรณ์มหาวิทยาลัย

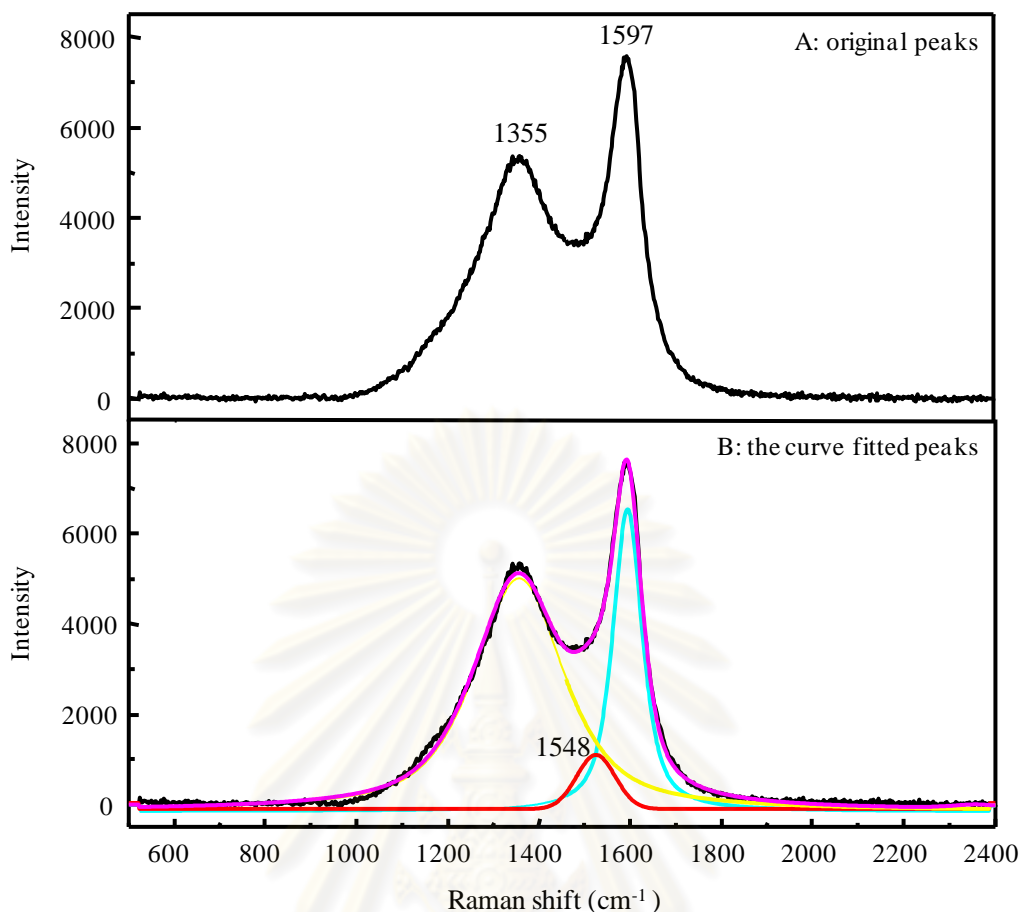


Figure 4.12 Raman spectra of CNPs with (A) original peaks and (B) the curve fitted peaks.

## 4.8.2 Morphology analysis/Imaging technique

### 4.8.2.1 Scanning electron microscopy (SEM)

CNPs samples were prepared by collecting them on aluminium plate by exposing to the soot. Figure 4.13A (insert) shows the image of CNPs film on aluminium plate, which was exposed to the soot for 2 seconds. Although, there is no significant changing on the surface of aluminium plate. When observing with SEM, the synthesized CNPs are deposited on the aluminium plate in the form of chain-like structure as shown in Figure 4.13A. Only monolayer of CNPs on the aluminium plate are found. This indicates that CNPs film is thin. If CNPs are collected by exposing to the soot for a longer time (30 seconds). As aforementioned earlier, Figure 4.13B (insert) shows that there is black soot on the surface of aluminium plate. When

observing with SEM, the synthesized CNPs depositing on the aluminium plate are still in the form of chain-like structure and there are many layers of CNPs on the aluminium plate as shown in Figure 4.13B. This indicates that CNPs film is thick. Additionally, the synthesized CNPs are collected from the aluminium plate as shown in Figure 4.13C (insert). The synthesized CNPs are ground before taking the SEM image. SEM image shows the bulky agglomerate of primary particles as shown in Figure 4.13C. Therefore, SEM image demonstrates that the synthesized CNPs are uniform spherical particles.

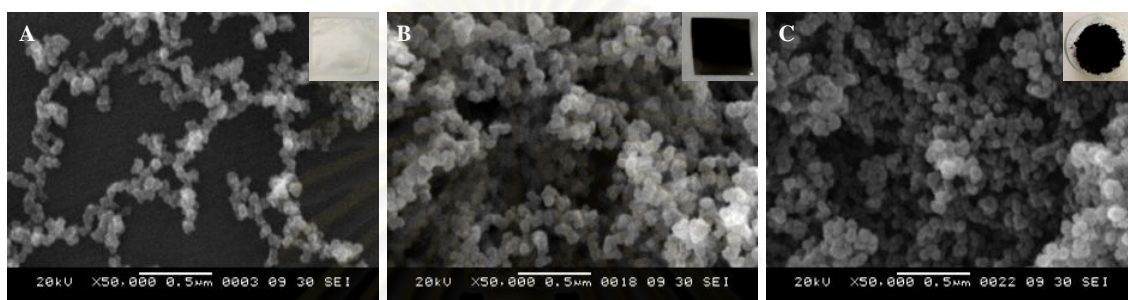


Figure 4.13 SEM images of CNPs: (A) CNPs thin film on aluminium plate, (B) CNPs thick film on aluminium plate, and (C) CNPs powder.

#### 4.8.2.2 Transmission electron microscopy (TEM)

The detailed particles size, particle size distribution, and particle agglomeration are exactly characterized by TEM. Figures 4.14A-4.14C show TEM images of the synthesized CNPs in correspondence with SEM image. There are many connected particles forming a chain-like structure and there are also uniform spherical particles. Figures 4.14D-4.14F show primary particles which can be separated to single particles after sonicating in ethanol for 1 hour. The synthesized CNPs have the spherical morphology. The average particles size of CNPs measured by ImageJ program with 100 particles is 49.70 nm. Histogram of the size of the synthesized CNPs suggests that CNPs have a range of particle size of 20–100 nm as shown in Figure 4.15.



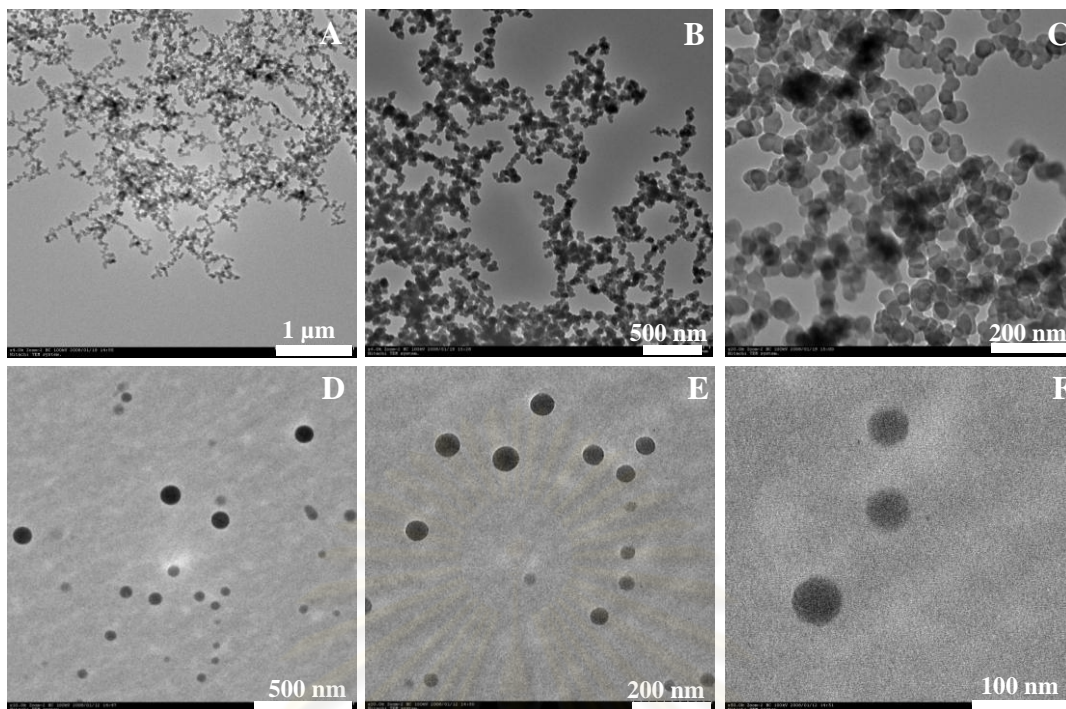


Figure 4.14 TEM images of CNPs: (A)–(C) chain like structure of CNPs, and (D)–(F) CNPs after ultrasonic in ethanol for 1 hour.

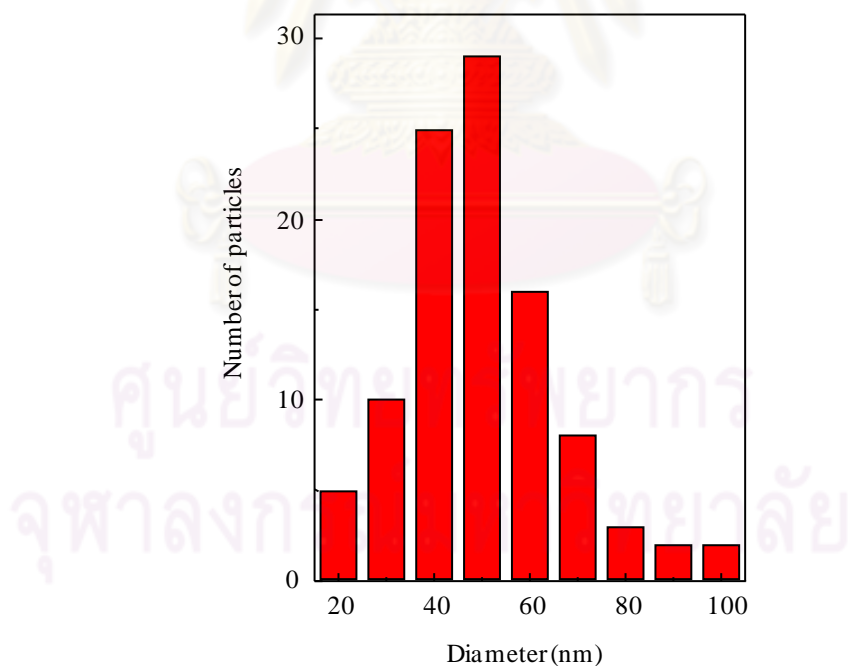


Figure 4.15 Histogram of the particle size of the synthesized CNPs by flame combustion technique.



### 4.8.2.3 Atomic force microscopy (AFM)

The synthesized CNPs are sonicated in ethanol for 1 hour before dropping on a cover glass. Due to the fact that the synthesized CNPs are soft and easily scraped, AFM in the dynamic force microscope mode (DFM) or non-contact mode is employed for acquiring surface topography, pattern of agglomeration, and particles size information of the synthesized CNPs. From AFM images shown in Figure 4.16 (A1) and (A2), CNPs are separated as the single particles. The black points on Figure 4.16 (A1) and (A2) are the air bubble hole of ethanol film which do not interfere the synthesized CNPs. This result is in good agreement with the result from TEM analysis. Figure 4.16 (B1) and (B2) show the synthesized CNPs collected by directly exposing the cover glass to the soot. The AFM image of CNPs film on cover glass corresponds with SEM image which is found that CNPs deposited on cover glass is still in the form of a chain-like structure. The primary particle of CNPs shown in Figure 4.16 (C1) and (C2) is the exact particles size before forming the chain-like structure. AFM images suggests that the synthesized CNPs are spherical and are in agreement with SEM and TEM images.

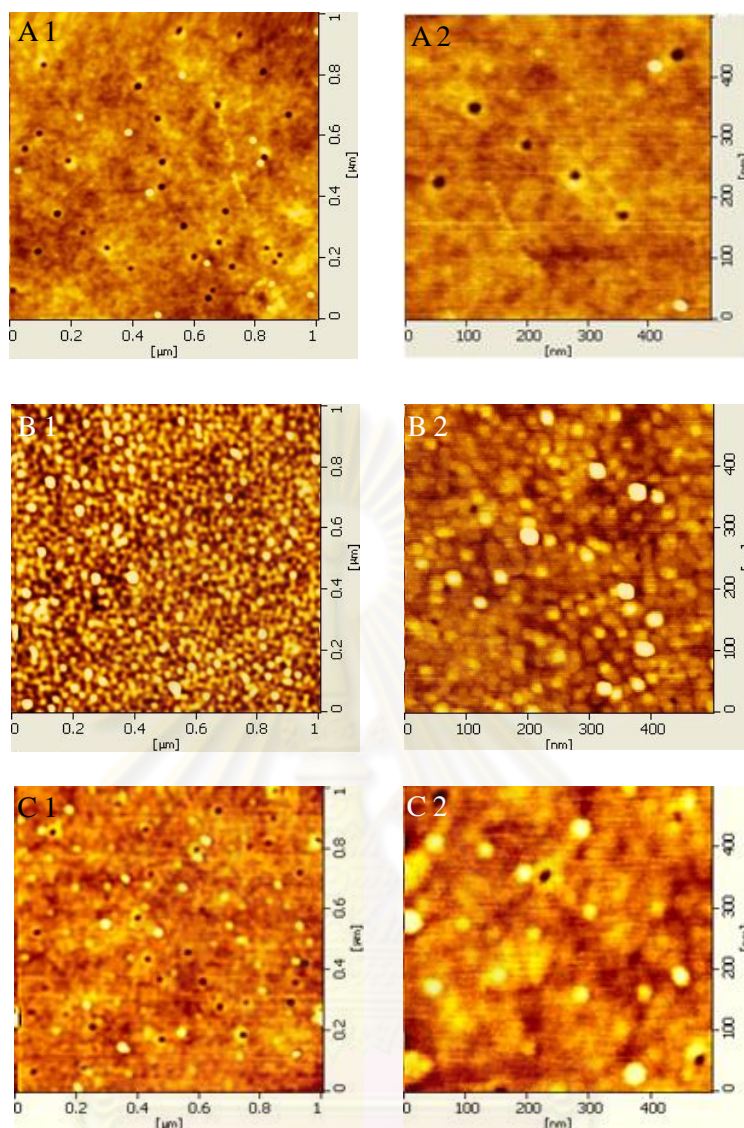


Figure 4.16 AFM images of CNPs after ultrasonication in ethanol ((A1) and (A2)), CNPs after exposing on cover glass directly to the soot ((B1) and (B2)), and CNPs after exposing the thin ethanol film coated on glass slide directly to the soot ((C1) and (C2)).

### 4.8.3 Surface area analysis

#### 4.8.3.1 N<sub>2</sub> adsorption/desorption analysis

The specific surface area of CNPs is determined by nitrogen adsorption/desorption analysis via the Brunauer–Emmett–Teller (BET) method which use to measure total surface area. The BET surface area shows a value of 95.05 m<sup>2</sup>/g, which is significantly higher than the reported value of synthesized CNPs of the same

particle size as shown in Table 4.6. Because the synthesized CNPs are loosely agglomerated, the measured surface area of CNPs is increased.

The theoretical surface area is calculated for amorphous and graphite structure in order to compare with the surface area of the synthesized CNPs. The density of various structures and diameter of the synthesized CNPs are used to calculate the theoretical surface area. The theoretical surface area of CNPs is calculated by:

$$S_{\text{sphere}} = \left(\frac{3m}{d}\right)^{\frac{2}{3}} \quad (4.1)$$

where,  $S_{\text{sphere}}$  = the surface area of a sphere ( $\text{m}^2$ )

$d$  = density of CNPs structure (e.g. amorphous, graphite) ( $\text{g}/\text{cm}^3$ )

Density of amorphous structure =  $1.8\text{-}2.1 \text{ g}/\text{cm}^3$  [34]

Density of graphite structure =  $2.2671 \text{ g}/\text{cm}^3$  [34]

$m$  = mass of a single CNPs (g)

Table 4.7 shows the theoretical surface area of the synthesized CNPs which consist of a minimum particle size of 20 nm and a maximum particle size of 100 nm of amorphous and graphite structure. The surface area is  $33.30\text{-}167.13 \text{ m}^2/\text{g}$  for amorphous structure. On the other hand, graphite structure has the surface area of  $26.45\text{-}131.95 \text{ m}^2/\text{g}$ . The surface area of the synthesized CNPs is in-between the surface area of amorphous and graphite structure. It suggests that the synthesized CNPs are the mixture of amorphous and graphite structures which this result is in good agreement with the results of XRD and Raman technique.

Table 4.6 The specific surface area comparisons of various particle size of CNPs.

Reference	Particle size of CNPs (nm)	Specific surface area (m <sup>2</sup> /g)
Sano, N. et. al. ( 2005 ) [38]	5	760
Serp, P. et.al. (2001) [39]	100-300	16.4
Wang, Y. et.al.(2008) [40]	40-50	59
This work	20-100	95.05

Table 4.7 The theoretical surface area of the synthesized CNPs.

Diameter of CNPs (nm)	The theoretical surface area (m <sup>2</sup> /g)
20 <sup>a</sup>	167.13
20 <sup>b</sup>	131.95
100 <sup>a</sup>	33.30
100 <sup>b</sup>	26.45

a: amorphous structure

b: graphite structure

#### 4.8.4 The volatile organic compound adsorption of CNPs

The synthesized CNPs are black powder and light weight. They must be casted to pellet in order to be easily utilized for the volatile organic compound adsorbing as shown in Figure 4.17A. The CNPs pellet (the diameter of 3.0 cm and the thickness of 1 mm) casting process is explained in CHAPTER III. Figure 4.17B shows the charcoal strip (commercial product) which is the sticky thin carbon plate (thickness = 0.5 mm). It is also employed in order to compare with our CNPs pellet in volatile organic compound adsorption efficiency.

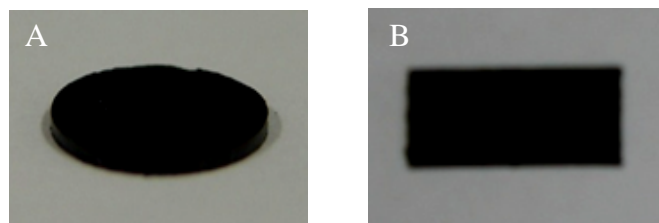


Figure 4.17 The volatile organic compound adsorber: (A) CNPs pellet and (B) the charcoal strip (commercial product).

#### 4.8.4.1 Adsorption of eucalyptus oil by CNPs pellet

Weight of CNPs powder and compression of hydraulic force were used to vary condition for CNPs pellet casting in order to get the optimal pellet as shown in Table 4.8. The optimal factors were the optimal pellet—no cracking of the CNPs pellet surface that are 0.1 g of CNPs powder, 1 Ton of compression force.

ATR FT–IR spectrum of CNPs pellet is shown in Figure 4.18A. There is no C–H stretching vibration at  $2,800\text{--}3,000\text{ cm}^{-1}$  and C–H bending vibration at  $1,350\text{--}1,480\text{ cm}^{-1}$  [29]. It suggests that CNPs pellet are pure carbon. The ATR FT–IR spectrum of eucalyptus oil is shown in Figure 4.18B. The molecular characteristics of adsorbed eucalyptus oil are clearly observed in the ATR FT–IR spectrum (Figure 4.18C) without any interference from the synthesized CNPs. This preliminary testing suggests that the synthesized CNPs have a potential application for the volatile organic compound adsorber.

Table 4.8 The result of CNPs pellet casting with various condition.

Weight of CNPs powder (g)	Compression (Ton)	CNPs pellet quality
0.05	0.5	CNPs pellet was cracked when applied compression force.
0.05	1.0	
0.05	2.0	
0.1	0.5	Condensed CNPs pellet without cracking.
0.1	1.0	
0.1	2.0	CNPs pellet was cracked when applied compression force.



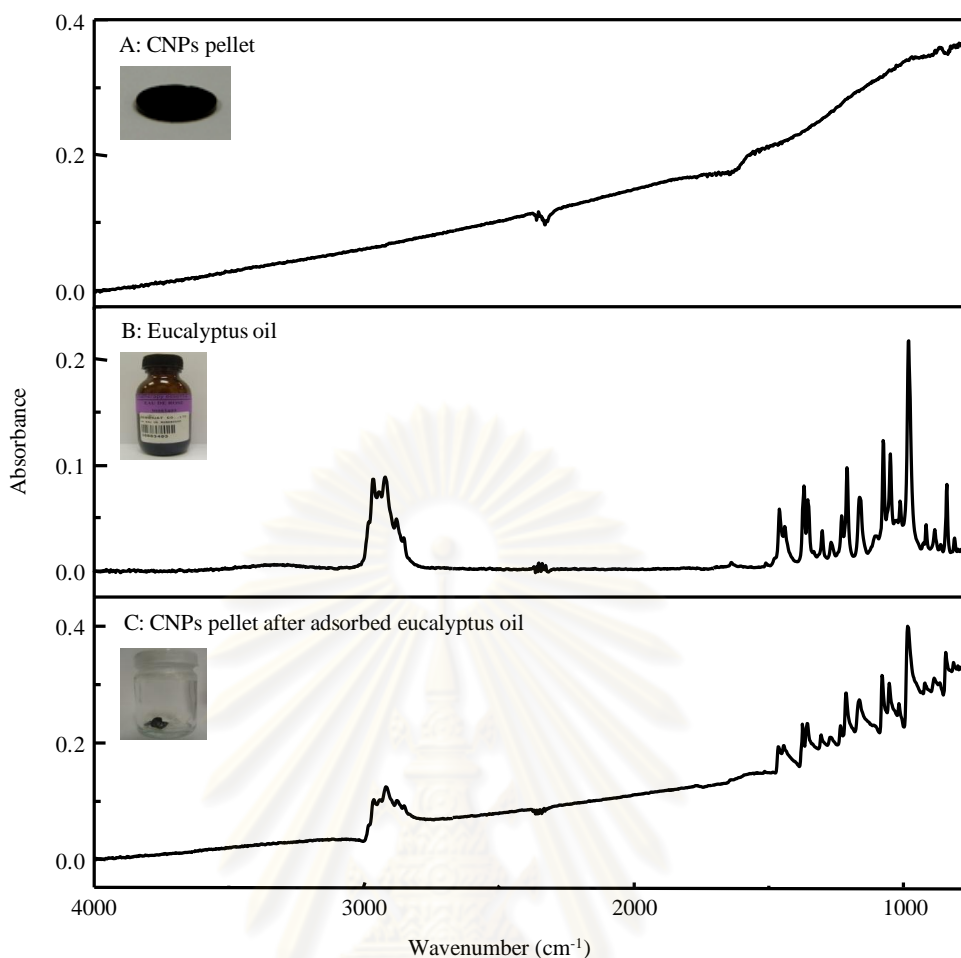


Figure 4.18 ATR spectra of (A) CNPs pellet, (B) eucalyptus oil, and (C) CNPs pellet with adsorbed-eucalyptus aroma.

#### 4.8.4.2 Adsorption of diesel oil by CNPs pellet

CNPs pellets casted for adsorption of eucalyptus oil were easily cracked. Therefore, the binder was added in CNPs pellet casting in order to strengthen it when utilized as volatile organic compound adsorber. The binders for mixing with CNPs powder were Teflon powder and a paper pulp which were not dissolved in dichloromethane (solvent in GC/FID test) as shown in Tables 4.9 and 4.10, respectively. The optimal binder was a paper pulp. When it was shaped, it was not cracked because a paper pulp has entanglement fiber. CNPs powder could penetrate into entanglement fiber. So, it was stronger than a Teflon powder binder. The optimal compression force was 1.5 Ton.



Table 4.9 The result of CNPs pellet casting with Teflon powder as binder.

Weight of CNPs powder (g)	Weight of Teflon powder (g)	Compression (Ton)	CNPs pellet quality
0.01	0.05	1.0	CNPs pellet easily cracked
0.01	0.05	1.0	
0.01	0.10	1.0	
0.01	0.10	1.5	
0.05	0.20	2.0	
0.05	0.20	2.5	
0.10	0.10	3.0	
0.10	0.05	1.5	

Table 4.10 The result of CNPs pellet casting with paper pulp as binder.

Weight of CNPs powder (g)	Weight of paper pulp (g)	Compression (Ton)	CNPs pellet quality
0.05	0.10	1.5	Condensed CNPs pellet with tolerable durability.
0.05	0.05	1.5	Brittle CNPs pellet
0.05	0.02	1.5	
0.05	0.01	2.0	
0.10	0.01	1.5	
0.10	0.01	1.0	
0.10	0.01	1.0	
0.10	0.01	1.0	

0.05 g of CNPs powder was mixed into 0.1 g of a paper pulp (Table 4.10). This ratio is chosen because, at too high CNPs content, CNPs pellet was cracked.

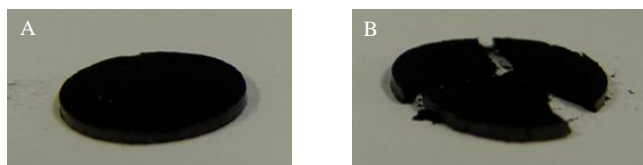


Figure 4.19 Feature of CNPs pellet: (A) condensed CNPs pellet with tolerable durability and (B) brittle CNPs pellet.

The experiment of diesel oil adsorption is performed in cooperation with Central Institute of Forensic Science (CIFS), Thailand. The diesel oil is commonly employed in arson crime. Arson is very difficult to prosecute due to the lack of biological evidence such as fingerprints, footprints, DNA etc., they are usually entirely destroyed by the fire, the heat, or covered with soot. So, the aim of the CIFS is to apply the activated charcoal for adsorption of flammable solvent residue—diesel oil. The CIFS used the commercially available charcoal strip in adsorption process. Chromatogram in Figure 4.20A shows the molecular characteristics of the commercial charcoal strip which do not have any impurity. However, there were the molecular characteristics of dichloromethane (solvent in the organic compound dissolving on charcoal strip). Chromatogram in Figure 4.20B shows the molecular characteristics of diesel oil which indicates the various element of compound in diesel oil. The first peak consisted of low boiling point compounds with rapid retention time (the evaporation time of compound in GC column). The last peak consisted of high boiling point compound with long retention time. In addition, the height of each peak depended on detector response. It indicates the quantity of each compound in diesel oil. The highest peak indicates that there is a lot of quantity of this compound in diesel oil. However, the flame ionization as detector was employed for the GC analysis. So, this chromatogram cannot suggest the name of each compound in diesel oil. However, it suggests molecular characteristics pattern of compound when compared with molecular characteristics pattern of standard compound or retention time of each compound peak of standard compound. Therefore, chromatogram of the adsorbed diesel oil on the charcoal strip show the molecular characteristic of diesel oil as shown in Figure 4.20C. It suggests that the charcoal strip has an efficiency for the volatile organic compound adsorber. But the commercial charcoal strip is expensive. The cheaper adsorber that is efficiently comparable to commercial product is preferable. Practically, the CIFS used CNPs pellet as the strip test adsorber. Figure 4.21A shows the molecular characteristics of our CNPs pellet which do not have any impurity. The adsorbed diesel oil on CNPs pellet indicates the molecular characteristic of diesel oil as shown in Figure 4.21C. It indicates that CNPs pellet have the same efficiency as that of the charcoal strip in the volatile organic compound adsorber. CNPs pellet is cheaper than that of the charcoal strip. Therefore, the synthesized CNPs have the prosperous tendency for the volatile organic compound adsorber.

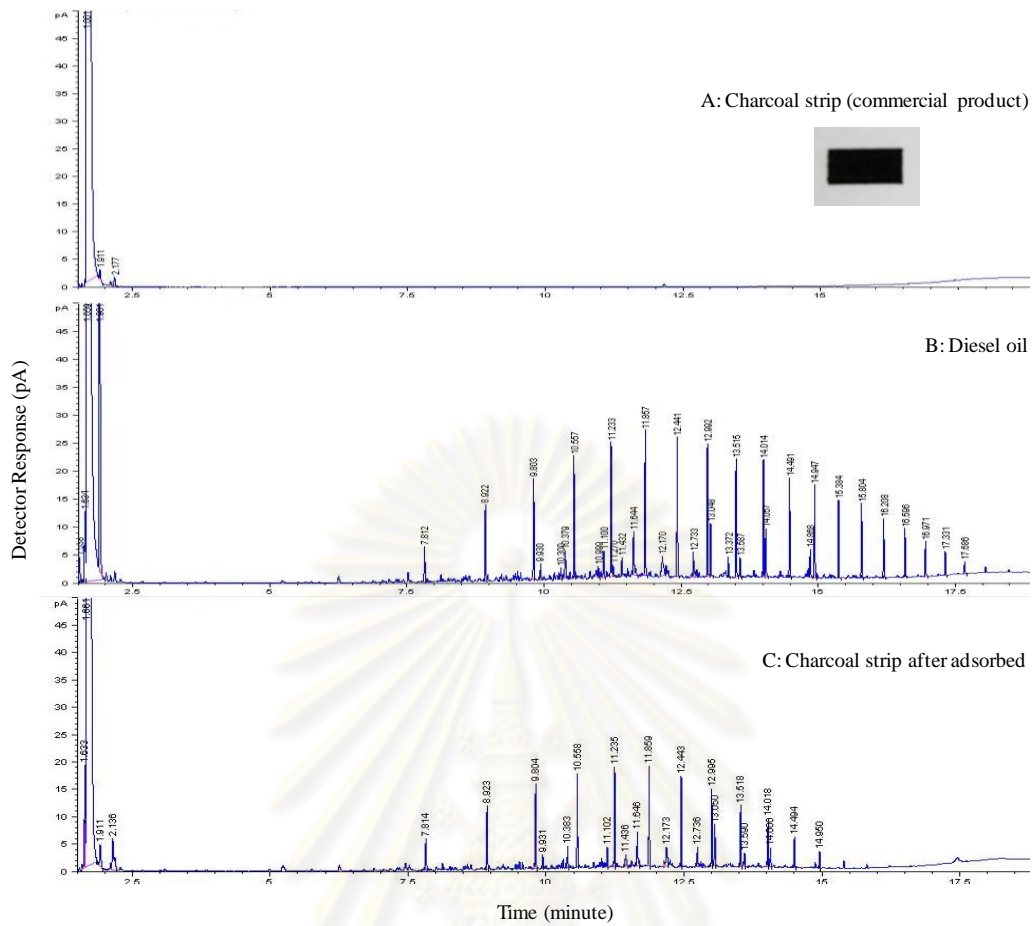


Figure 4.20 GC peaks of (A) charcoal strip (commercial product), (B) diesel oil, and (C) charcoal strip with adsorbed–diesel oil.

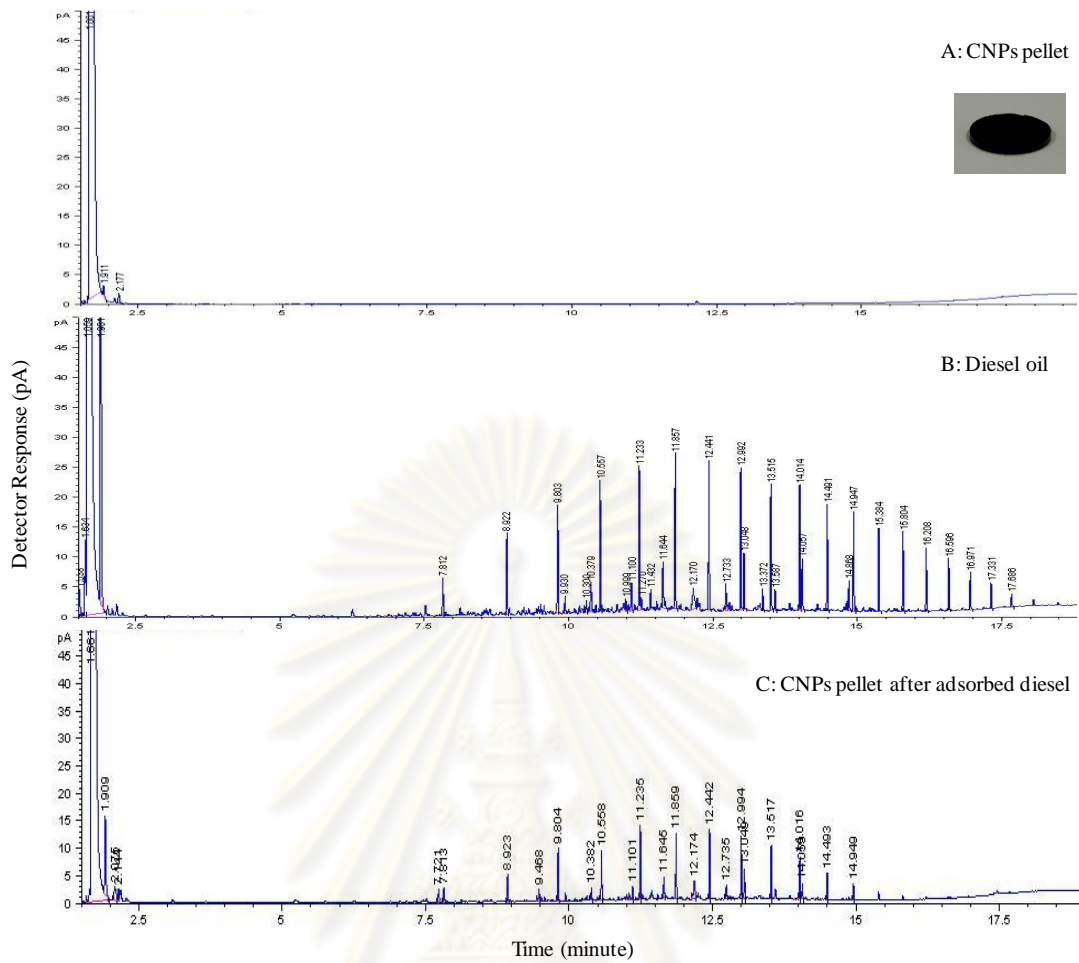


Figure 4.21 GC peaks of (A) CNPs pellet, (B) diesel oil, and (C) CNPs pellet with adsorbed–diesel oil.

## CHAPTER V

### CONCLUSIONS

It is concluded that CNPs can be synthesized by a simple technique using paraffin combustion in the form of candle and employed as a carbon source. These CNPs can be utilized as an adsorber of volatile organic compound.

Synthesis of CNPs was affected by the various factors. The optimal factors are the ratio of diameter size of candle wick and candle wax body is 0.5:2, the candle flame disturbance has carried out between the fourth and the fifth zone, the mesh grid interval is 0.1 cm, the wire for the grid weaving is nichrome wire and the grid shape is square shape. These optimal factors gave the highest yield of CNPs and pure CNPs.

ATR FT-IR spectra of CNPs reveal no C-H stretching vibration of wax at 2,800–3,000  $\text{cm}^{-1}$  and C-H bending vibration at 1,350-1,480  $\text{cm}^{-1}$ . It has C=C stretching vibration of carbon at 1,580  $\text{cm}^{-1}$ . This implies that the CNPs is pure without any interference of wax. The synthesized CNPs are the combination of disorder graphite, graphite, and an amorphous structure. The obtained spherical CNPs have particle size of 20-100 nm. CNPs are chain-like structures which are loosely agglomerated. The BET surface area shows a value of 95.05  $\text{m}^2/\text{g}$  which is significantly higher than the reported value of the synthesized CNPs for a similar particle size.

CNPs can be applied as a volatile organic compound adsorber. The molecular characteristics of adsorbed eucalyptus oil and diesel oil (The cooperative testing with Central Institute of Forensic Science, CIFS) clearly reveal the molecular characteristics of eucalyptus oil and diesel oil on CNPs pellet. It has no interference from the synthesized CNPs. Therefore, the synthesized CNPs can be utilized as an adsorber of volatile organic compound.

This synthesis technique can produce a few quantity of CNPs. However, the synthesized CNPs are pure and have high surface area. In the future, the apparatus for synthesizing the CNPs will be improved. The close and stagnant system will also be incorporated. The synthesized CNPs have the high potential for developing as sensor for superadsorber, catalyst supporting substances, and filler.

## REFERENCES

- [1] Liu, H.; Ye, T.; and Mao, C. Fluorescent Carbon Nanoparticles Derived from Candle Soot. Angew. Chem. Int Ed. 46 (2007): 6473-6475.
- [2] Yan, A.; Lau, W. B.; Kulaots, I.; Yang, Y. C. N.; Kane, B. A.; and Hurt, H. R. Biocompatible, Hydrophilic, Supramolecular Carbon Nanoparticles for Cell Delivery. Adv. Mater. 18 (2006): 2373–2378.
- [3] Chen, G.X.; Hong, M.H.; He, Q.; Chen, W.Z.; Elim, H.I.; Ji, W.; Chong, T.C. Formation, structure and nonlinear optical properties of carbon nanoparticles synthesized by pulsed laser ablation. Appl. Phys. A79 (2004): 1079-1082.
- [4] Yu, J.; Zhang, Q.; Ahn, J.; Yoon, S.F.; Rusli; Li, Y.J.; Gan, B.; Chew, K. Synthesis of carbon nanoparticles by Microwave Plasma Chemical Vapor Deposition and Their Field Emission Properties. J. Mater. Sci. 21 (2002): 543-545.
- [5] Charinpanitkul, T.; Tanthapanichakoon W.; and Sano, N. Carbon Nanostructure Synthesized by Arc Discharge between Carbon and Iron Electrodes in Liquid Nitrogen. Curr. Appl. Phys. 9 (2008): 629-632.
- [6] Jin, Z.Y.; Gao, C.; Hsu, K.W.; Zhu, Y.; Huczko, A.; Bystrzejewski, M.; Roe, M.; Lee, Y.C.; Acquah, S; Kroto, H.; and Walton, R.M.D. Large-scale Synthesis and Characterization of Carbon Spheres prepared by Direct Pyrolysis of Hydrocarbons. Carbon. 43 (2005): 1944-1953.
- [7] Naha, S.; Sen, S.; and Puri, K.I. Flame Synthesis of Superhydrophobic Amorphous Carbon Surfaces. Carbon. 45 (2007): 1696-1716.
- [8] Nelsen, W.L. Petroleum Refinery Engineering. 4<sup>th</sup> ed. Singapore: McGraw-Hill, 1985.
- [9] Hamins, A.; and Bundy, M. Characterization of Candle Flames. J. Fire Prot. Eng. 15 (2005): 265-284.
- [10] Walker, J. The Physics and Chemistry Underlying the Infinite Charm of a Candle Flame. New York, 1978.
- [11] Faraday, M. The Chemical History of Candle. New York: The Viking Press, 1960.



- [12] Seeker, Z. How Backpacking Stoves Work. [online]. Available from: <http://zenstoves.net/How.htm>
- [13] Mishra, D.P. Fundamentals of Combustion. New Delhi: Prentice-Hall of India Private Limited, 2008.
- [14] Setten, V., L., A., A., B.; Makkee, M.; and Moulijn, A., J. Science and Technology of Catalytic Diesel Particulate Filters. Catal. Rev. 43(2001): 489-564.
- [15] Ishiguro, T.; Takatori, Y.; and Akihama, K. Microstructure of Diesel Soot Particles Probed by Electron Microscopy: First Observation of Inner Core and Outer Shell. Combust. Flame. (108) 1997: 231-234.
- [16] Inagaki, M. Discussion of the Formation of Nanometric Texture in Spherical Carbon Bodies. Carbon. 35 (1997): 711-713.
- [17] Serp, Ph.; Feurer, R.; Kalck, Ph.; Kihn, Y.; Faria, J.L.; and Figueiredo, J.L. A Chemical Vapour Deposition Process for the Production of Carbon Nanospheres. Carbon. 39 (2001): 615-628.
- [18] Quercia, L.; Loffredo, F; Alfano, B; Ferrara, V., L.; Francia, G, D. Fabrication and characterization of Carbon Nanoparticles for Polymer Based Vapor Sensor Sensor.Actuat. B-Chem. 100 (2004): 22-28.
- [19] Ozawa, M.; and Osawa, E. Carbon Black as the Source Material for Carbon Nanotechnology, Carbon Nanotechnology, 127-151. Japan: Elsevier, 2006.
- [20] Wang, Y.; Su, F.; Wood, D.C.; Lee, Y.J.; and Zhao, S.X. Preparation and Characterization of Carbon Nanospheres as Anode Materials in Lithium-Ion Secondary Batteries. Ind. Eng. Chem. Res. 47 (2008): 2294-2300.
- [21] Sharon, M.; and Sharon, M. Carbon Nanomaterials: Applications in Physico-chemical Systems and Biosystems. Defence. Sci. J. 58 (2008): 460-485.
- [22] Kammler, K.H.; Mädler L.; and Pratsinis, E.S. Flame Synthesis of Nanoparticles. Chem. Eng. Technol. 24 (2001): 583-595.
- [23] Do, T. T.; Celina, M.; and Fredericks, P. Attenuated Total Reflectance Infrared Microspectroscopy of Aged Carbon-filled Rubbers. Polym. Degrad. Stab. 77 (2002): 417-422.
- [24] Skoog, A.D.; and Leary, J.J. Principles of Instrumental Analysis. 4<sup>th</sup> ed. The United States of America: Saunders College Publishing, 1992.
- [25] Willard, H.H.; Merritt, L.L.; and Dean, A.J. Instrumental Methods of Analysis. 5<sup>th</sup> ed. New York: D. Van Nostrand Company, 1974.

- [26] Robert, K.; Ian, H.; and Mark, G. Nanoscale Sci. & Tech. Wiley copyright, 2005.
- [27] Jalili, N.; and Laxminarayana, K. A Review of Atomic Force Microscopy Imaging Systems: Application to Molecular Metrology and Biological Sciences. Mechatronics. 14 (2004): 907-945.
- [28] Brunauer, S.; Emmett, P.M.; and Teller, E. Adsorption of Gases in Multimolecular Layers. J. Am. Chem. Soc. 60 (1938): 309–319.
- [29] Socrates, G. Infrared and Raman Characteristic Group Frequencies Tables and Charts. New York : John Wiley & Sons Ltd, 2001.
- [30] Llamas-Jansa, I.; Jager, C.; Mutschke, H.; and Henning, Th. Far-Ultraviolet to Near-infrared Optical Properties of Carbon Nanoparticles produced by Pulsed-laser Pyrolysis of Hydrocarbons and their Relation with Structural Variations. Carbon. 45 (2007): 1542-1557.
- [31] Inagaki, M.; and Feiyu, K. Carbon Materials Science and Engineering: From Fundamentals to Applications. China: Tsinghua University Press, 2006.
- [32] Humecki, H. J. Practical Guide to Infrared Microspectroscopy. New York: Marcel Dekker, 1995.
- [33] Cengel, A., Y., Turner, H., R., and Cimbala, M., J. Fundamentals of thermal-fluid science. Singapore: McGraw-Hill, 2008.
- [34] Fey, T.-K., G.; Lee, D.C.; Lin, Y.Y.; and Kumar, P., T. High-capacity Disordered Carbons Derived from Peanut Shells as Lithium-intercalating Anode Materials. Synthmet. 139 (2003): 71-80.
- [35] Yi, Z.; Liang, Y.; Lei, X.; Wang, C.; and Sun, J. Low-temperature Synthesis of Nanosized Disorder Carbon Spheres as an Anode Material for Lithium Ion Batteries. Matlet. 61 (2007): 4199-4203.
- [36] Jawhari, T.; Roid, A.; and Casado, J. Raman Spectroscopic Characterization of some Commercially Available Carbon Black Materials. Carbon. 33 (1995): 1561-1565.
- [37] Pierson, O.H. Handbook of Carbon Graphite, Diamond and Fullerenes Properties, Processing and Applications. The United States of America: Noyes Publications, 1993.
- [38] Sano, N.; Wang, H.; Alexandrou, I; Chhowalla, M.; Teo, K.B.K.; and Amaratunga, J.A.G. Properties of Carbon Onions Produced by an Arc Discharge in Water. J. Appl. Phys. 92 (2002): 2783-2788.

- [39] Serp, Ph.; Feurer, R.; Kalck, Ph.; Kihn, Y.; Faria, J.L.; and Figueiredo, J.L. A Chemical Vapour Deposition Process for the Production of Carbon Nanospheres. Carbon. 39 (2001): 615-628.
- [40] Wang, Y.; Su, F.; Wood, D.C.; Lee, Y.J.; and Zhao, S.X. Preparation and Characterization of Carbon Nanospheres as Anode Materials in Lithium-Ion Secondary Batteries. Ind. Eng. Chem. Res. 47 (2008): 2294-2300.



ศูนย์วิทยทรัพยากร  
จุฬาลงกรณ์มหาวิทยาลัย



## **APPENDIX**

ศูนย์วิทยทรัพยากร  
จุฬาลงกรณ์มหาวิทยาลัย

### 1. The % yield of CNPs calculation

$$\% \text{ yield} = \frac{W_c(\text{g})}{W_p(\text{g})} \times 100$$

$$W_p(\text{g}) = W_{p_i}(\text{g}) - W_{p_f}(\text{g})$$

where  $W_c$  is the weight of synthesized CNPs,  $W_p$  is the weight of the used paraffin in the synthesis,  $W_{p_i}$  is the initial weight of paraffin (g), and  $W_{p_f}$  is the final weight of paraffin (g)

For example;

The synthesis of CNPs by candle wick

Initial weight of paraffin ( $W_{p_i}$ )	=	35.487 g
Final weight of paraffin ( $W_{p_f}$ )	=	31.239 g
Weight of the synthesized CNPs ( $W_c$ )	=	0.045 g
Weight of the used paraffin in the synthesis ( $W_p$ )	=	$35.487 - 31.239 = 4.248 \text{ g}$

$$\% \text{ yield} = \frac{0.045}{4.248} \times 100 = 1.05$$

Therefore, % yield of CNPs is equal to 1.05.

### 2. The standard deviation (S) of the %yield

$$S = \sqrt{\frac{1}{n-1} \sum_{i=1}^n (X_i - \bar{X})^2}$$

where,  $X_i$  = one value in data setting,  $\bar{X}$  = the mean (average) of all values  $X_i$ , and  $n$  = the number of values  $x$  in data setting

For example,

% yield of CNPs consists of three data are 1.05, 1.03 and 1.07.

$$\bar{X} = 1.05, n = 3$$

The standard deviation is

$$S = \sqrt{\frac{(1.05-1.05)^2 + (1.03-1.05)^2 + (1.07-1.05)^2}{(3-1)}} = 0.02$$

Therefore, % yield of CNPs = 1.05±0.02

### 3. The yield of the synthesis CNPs from small candle wick

Times	Weight of paraffin before burning (g)	Weight of paraffin after burning (g)	Weight of paraffin (g)	Weight of carbon (g)	% Yield of carbon
1	35.487	31.239	4.248	0.045	1.05
2	37.156	33.095	4.061	0.042	1.03
3	39.283	35.012	4.271	0.046	1.07

### 4. The yield of the synthesis CNPs from big candle wick

Times	Weight of paraffin before burning (g)	Weight of paraffin after burning (g)	Weight of paraffin (g)	Weight of carbon (g)	% Yield of carbon
1	38.682	35.186	3.496	0.072	2.06
2	35.561	32.101	3.460	0.070	2.02
3	39.543	36.124	3.419	0.071	2.07



**5. The yield of the synthesis CNPs from grid interval of 1.0 cm**

Times	Weight of paraffin before burning (g)	Weight of paraffin after burning (g)	Weight of paraffin (g)	Weight of carbon (g)	% Yield of carbon
1	57.650	52.656	4.994	0.033	0.66
2	56.987	52.091	4.896	0.036	0.74
3	57.262	52.337	4.925	0.034	0.69

**6. The yield of the synthesis CNPs from grid interval of 0.5 cm**

Times	Weight of paraffin before burning (g)	Weight of paraffin after burning (g)	Weight of paraffin (g)	Weight of carbon (g)	% Yield of carbon
1	61.245	56.201	5.044	0.051	1.01
2	62.056	56.941	5.115	0.053	1.04
3	62.567	57.482	5.085	0.052	1.02

**7. The yield of the synthesis CNPs from grid interval of 0.1 cm**

Times	Weight of paraffin before burning (g)	Weight of paraffin after burning (g)	Weight of paraffin (g)	Weight of carbon (g)	% Yield of carbon
1	38.733	35.220	3.513	0.073	2.08
2	36.560	33.278	3.282	0.068	2.07
3	37.825	34.454	3.471	0.071	2.13

**8. The yield of the synthesis CNPs from copper wire for the grid weaving**

Times	Weight of paraffin before burning (g)	Weight of paraffin after burning (g)	Weight of paraffin (g)	Weight of carbon (g)	% Yield of carbon
1	60.334	54.167	6.167	0.125	2.03
2	62.561	56.064	6.497	0.135	2.08
3	65.214	58.972	6.242	0.131	2.10

**9. The yield of the synthesis CNPs from iron wire for the grid weaving**

Times	Weight of paraffin before burning (g)	Weight of paraffin after burning (g)	Weight of paraffin (g)	Weight of carbon (g)	% Yield of carbon
1	59.893	53.436	6.457	0.132	2.04
2	56.758	49.926	6.832	0.143	2.09
3	60.158	54.033	6.125	0.126	2.06

**10. The yield of the synthesis CNPs from nichrome wire for the grid weaving**

Times	Weight of paraffin before burning (g)	Weight of paraffin after burning (g)	Weight of paraffin (g)	Weight of carbon (g)	% Yield of carbon
1	59.580	55.204	4.376	0.158	3.61
2	57.691	52.807	4.884	0.180	3.69
3	62.145	56.663	5.482	0.201	3.67

### 11. The yield of the synthesis CNPs from square grid shape

Times	Weight of paraffin before burning (g)	Weight of paraffin after burning (g)	Weight of paraffin (g)	Weight of carbon (g)	% Yield of carbon
1	59.580	55.204	4.376	0.158	3.61
2	57.691	52.807	4.884	0.180	3.69
3	62.145	56.663	5.482	0.201	3.67

### 12. The yield of the synthesis CNPs from dome grid shape

Times	Weight of paraffin before burning (g)	Weight of paraffin after burning (g)	Weight of paraffin (g)	Weight of carbon (g)	% Yield of carbon
1	54.578	48.362	6.216	0.163	2.62
2	56.937	50.738	6.199	0.162	2.61
3	54.619	48.383	6.236	0.171	2.65

### 13. The theoretical surface area of CNPs calculation

1. Determine the volume of sphere per one particle ( $v_{\text{sphere}}$ ) from

$$v_{\text{sphere}} = \frac{4}{3} \pi r^3 (\text{cm}^3)$$

2. Substitute  $v_{\text{sphere}}$  into the density formula in order to calculate mass

$$d = \frac{m(\text{g})}{v_{\text{sphere}} (\text{cm}^3)}$$

where,  $d$  = density of CNPs structure (e.g. amorphous, graphite),  $\text{g/cm}^3$

Density of amorphous structure =  $1.8\text{-}2.1 \text{ g/cm}^3$  [34]

Density of graphite structure =  $2.2671 \text{ g/cm}^3$  [34]

$m$  = mass of CNPs per one particle, g

3. Determine the number of 1 g CNPs from

$$B \text{ (number of particle/g)} = \frac{1}{A \text{ (g)}}$$

where, B = the number of 1 g CNPs, number of particle/g  
A = weight of 1 particle of CNPs, g/particle

4. Determine the surface area of 1 particle of CNPs from

$$S_{\text{sphere}} = 4\pi r^2 \text{ (m}^2\text{)}$$

where,  $S_{\text{sphere}}$  = the surface area of a sphere,  $\text{m}^2/\text{particle}$   
r = radius of a sphere, m

5. Determine the theoretical surface area of CNPs from

$$C \text{ (m}^2\text{/g)} = B \text{ (number of particle/g)} \times S \text{ (m}^2\text{/particle)}$$

where, C = the surface area of CNPs,  $\text{m}^2/\text{particle}$

B = the number of 1 g CNPs, number of particle/g

S = the surface area of a sphere,  $\text{m}^2/\text{particle}$

จุฬาลงกรณ์มหาวิทยาลัย

#### 14. The synthesized CNPs cost

The material in CNPs synthesis	A cost (Baht)
1. Paraffin wax 15.50 g	1.55
2. Candle wick one piece (a length of 15 cm)	2.00
3. The nichrome wire for grid weaving (3.00 m)	120.00
4. Aluminium plate (0.50 m)	25.00
5. Paper pulp for binder in pellet casting (0.10 g)	0.0032
<b>Total</b>	<b>148.55</b>

Therefore, a cost of one CNPs pellet equals 148.55 Baht which was cheaper than a cost of commercial product (charcoal strip has a cost of 500 Baht).

## VITAE

**Name:** Miss Yaowapa Sarajan

**Date of Birth:** March 21, 1985                      **Birth place:** Roi-Et, Thailand

**Address:** 61/36, Moo 7, Tambon Bang Kraso, Amphoe Mueangnonthaburi,  
Nonthaburi 11000, Thailand

E-mail address: harry\_meaw@hotmail.com

### Education:

2007 Bachelor of Chemistry, Faculty of Science, King Mongkut's  
University of Technology Thonburi, Bangkok, Thailand

2009 Master of Science (Petrochemistry and Polymer Science),  
Chulalongkorn University, Bangkok, Thailand

### Conferences:

June 2008 Yonsei University–Chulalongkorn University, The 2<sup>nd</sup> Joint  
Symposium, Dept. of Chemistry Yonsei University, Seoul, Korea

November 2008 The 34<sup>th</sup> Congress on Science and Technology Thailand  
(STT 34), Bangkok, Thailand

December 2008 The 4<sup>th</sup> Mathematic and Physical Science Graduate Conference  
(MPSGC), Faculty of Science, National University of Singapore,  
Singapore

January 2009 Pure and Applied Chemistry International Conference 2009  
(PACCON 2009), Naresuan University, Phitsanulok, Thailand

March 2009 The Science Forum 2009, Chulalongkorn University, Bangkok,  
Thailand

May 2009 The 2<sup>nd</sup> Polymer Graduate Conference of Thailand, Faculty of  
Science, Chulalongkorn University, Thailand